



1 **Impact of Athabasca oil sands operations on mercury levels in air and deposition**

2

3 Ashu Dastoor¹, Andrei Ryjkov¹, Gregor Kos², Junhua Zhang³, Jane Kirk⁴, Matthew Parsons⁵ and
4 Alexandra Steffen³

5 ¹Air Quality Research Division, Environment and Climate Change Canada, 2121 Trans-Canada
6 Highway, Dorval, Québec, Canada

7 ²Department of Chemistry and Biochemistry, Concordia University, 7141 Sherbrooke Street
8 West, Montreal, Québec, Canada

9 ³Air Quality Research Division, Environment and Climate Change Canada, 4905 Dufferin Street,
10 Toronto, Ontario, Canada

11 ⁴Aquatic Contaminants Research Division, Environment and Climate Change Canada, 867
12 Lakeshore Road, Burlington, Ontario, Canada

13 ⁵Meteorological Service of Canada, Environment and Climate Change Canada, 9250 49 Street
14 NW, Edmonton, Alberta, Canada

15

16 **Correspondence:** Ashu Dastoor (ashu.dastoor@canada.ca)

17

18 **Abstract**

19 Oil sands upgrading facilities in the Athabasca Oil Sands Region (AOSR) in Alberta, Canada, have
20 been reporting mercury (Hg) emissions to public government databases (National Pollutant
21 Release Inventory (NPRI)) since the year 2000, yet the relative contribution of these emissions to
22 ambient Hg deposition remains unknown. A 3D process-based global Hg model, GEM-MACH-
23 Hg, was applied to simulate the Hg burden in and around the AOSR using NPRI reported oil sands
24 Hg emissions from 2012 (59 kg) to 2015 (25 kg) and other regional and global Hg emissions. The
25 impact of oil sands emissions (OSE) on Hg levels in the AOSR, relative to contributions from
26 sources such as global anthropogenic and biomass burning emissions (BBE), was assessed. In
27 addition, the relative importance of year-to-year changes in Hg emissions from the above sources
28 and meteorological conditions to inter-annual variations in Hg deposition was examined. Model
29 simulated surface air concentrations of Hg species and annually accumulated Hg in snowpacks
30 were found comparable to independently obtained measurements in the AOSR, suggesting
31 consistency between reported Hg emissions from oil sands activities and Hg levels in the region.



32 As a result of global-scale transport of gaseous elemental Hg (Hg(0)), surface air concentrations
33 of Hg(0) in the AOSR reflected the background Hg(0) levels in Canada (1.4 ng m^{-3} , AOSR;
34 $1.2\text{-}1.6 \text{ ng m}^{-3}$, Canada) with negligible impact from OSE. Highly spatiotemporally variable
35 wildfire Hg emission events led to episodes of high ambient Hg(0) air concentrations of up to 2.5
36 ng m^{-3} during the burning season. By comparison, average air concentrations of total oxidised Hg
37 (gaseous plus particulate; efficiently deposited Hg species) in the AOSR were elevated by 60%
38 above background levels (2012-2013) within 50 km of the oil sands major upgraders as a result of
39 OSE. Annual average Hg deposition fluxes in the AOSR were within the range of the deposition
40 fluxes measured for the entire province of Alberta ($15.6\text{-}18.3 \mu\text{g m}^{-2}\text{y}^{-1}$, AOSR (2012-2015); $\sim 14\text{-}$
41 $25 \mu\text{g m}^{-2}\text{y}^{-1}$, Alberta (2015)). Winter (November-April) and summer (June-August), respectively,
42 accounted for 20% and 50% of the annual Hg deposition in the AOSR. On a broad spatial scale,
43 imported Hg from global sources dominated the annual Hg deposition in the AOSR, with present-
44 day global anthropogenic emissions contributing to 40% ($< 1\%$ from Canada excluding OSE), and
45 geogenic emissions and re-emissions of legacy mercury deposition contributing to 60% of the
46 background Hg deposition. Further, wildfire events contributed to regional Hg deposition with
47 enhancements of 1-13% across 200 km range of major oil sands sources. In contrast, oil sands Hg
48 emissions were responsible for significant Hg deposition enhancements in the immediate vicinity
49 of oil sands Hg emission sources, up to 100 km in winter and up to 30 km in summer. Hg deposition
50 enhancements related to oil sands emissions were about 10 times larger in winter than summer
51 (average enhancement of 250 – 350% in winter and $\sim 35\%$ in summer within 10 km of OSE, 2012-
52 2013). In addition, snowpack Hg loadings and wintertime Hg deposition displayed significantly
53 higher inter-annual variations compared to summertime deposition due to changes in
54 meteorological conditions (such as precipitation amounts, wind speed, surface air temperature,
55 solar insolation, and snowpack dynamics) as well as oil sands emissions. For example, a large
56 snowmelt event at the end of February in 2015 effectively removed about half of the accumulated
57 mercury in snow, contributing to (observed and modeled) low annual snow Hg loadings. Inter-
58 annual variations in meteorological conditions were found to both exacerbate and diminish the
59 impacts of OSE on Hg deposition in the AOSR, which can confound the interpretation of trends
60 in short-term environmental Hg monitoring data. In winter, within 10 km of major oil sands
61 sources, variations in meteorology led to Hg deposition reduction by 17% in 2014 and increase by
62 10% in 2015 and decline in OSE lowered Hg deposition by 35% (2014) and 56% (2015), resulting



63 in overall reductions in wintertime Hg deposition of 52% (2014) and 46% (2015), relative to 2012.
64 By comparison, annually, changes in meteorology and BBE in 2014-2015 (relative to 2012) led to
65 Hg deposition increases of 1-6% and 2%, respectively, and decline in OSE lowered deposition by
66 15-22%, resulting in overall reduction in Hg deposition of 7-20% within 10 km of oil sands
67 sources. Hg runoff in spring flood, comprising the majority of annual Hg runoff, is mainly derived
68 from seasonal snowpack Hg loadings and mobilization of Hg deposited in surface soils, both of
69 which are sensitive to Hg emissions from oil sands developments in proximity of sources. Model
70 results suggest that sustained efforts to reduce anthropogenic Hg emissions from both global and
71 oil sands sources are required to reduce Hg deposition in the AOSR.

72

73 **Introduction**

74 Mercury (Hg) is a toxic element that accumulates in fish and mammals near the top of the food
75 web, including humans (e.g., through consumption of contaminated fish), where it exhibits long-
76 term toxic effects (UNEP, 2018). Hg is emitted to the atmosphere from geogenic sources such as
77 volcanoes and the weathering of Hg-containing rocks, anthropogenic sources such as fossil fuel
78 burning, metal smelting and artisanal gold mining, and through the re-emission of Hg historically
79 deposited from anthropogenic and natural sources onto soils, surface waters, and vegetation
80 (UNEP, 2013). Atmospheric Hg exists mainly in three forms: gaseous elemental mercury (Hg(0)
81 or GEM), gaseous oxidized mercury (gaseous Hg(II); GOM), and particle bound mercury (particle
82 bound Hg(II); PBM). The sum of GOM and PBM is referred to as total oxidised mercury (TOM)
83 and the sum of gaseous mercury species (i.e., GEM and GOM) is referred to as total gaseous
84 mercury (TGM) in this study. GEM/TGM and TOM are better indicators to compare observation
85 and model estimates of mercury for the purpose of this study, because of speciation uncertainties
86 associated with the determination of GOM and PBM species (Gustin et al., 2013). Deposition of
87 atmospheric Hg species by rain and snow (i.e., wet deposition), and by interfacial uptake on
88 various surfaces such as soils, vegetation, water, and snowpack (i.e., dry deposition) are the
89 pathways that contribute to Hg loadings in ecosystems. Typically, atmospheric GEM
90 concentrations are found to be 2-3 orders of magnitude higher (in the low ng m^{-3} range) than GOM
91 and PBM (typically in the lower pg m^{-3} range) because GEM is the dominant atmospheric Hg
92 species emitted to air and the reactivity of the latter (GOM and PBM) leads to efficient dry and
93 wet deposition removal of these species close to sources. Stability and volatility of GEM results



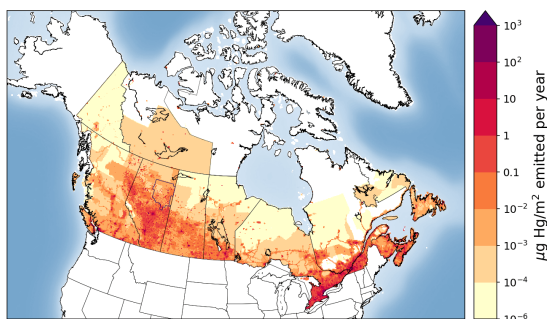
94 in its long lifetime in the atmosphere, with six months to one year, allowing for transport and
95 distribution on a global scale, and re-emission from planetary surfaces (UNEP, 2013).

96

97 On a global scale, dry deposition of GEM by vegetation-uptake over land and wet deposition of
98 TOM produced by atmospheric oxidation of GEM are the dominant pathways of Hg removal
99 (Obrist et al. 2016; Wright et al., 2016; Zhou et al. 2021). Primary emissions of GOM and PBM
100 from industrial sources are an important contributor to dry and wet depositions of Hg on a local to
101 regional scale. Once Hg is deposited to surfaces, it can be reduced and re-emitted back as GEM to
102 the air and, thus, Hg redistributes and accumulates in the aquatic and terrestrial environments
103 globally. Hg also inhibits enzymatic processes and reacts with organic compounds. This leads to
104 the formation of toxic, and bioaccumulating, methyl-Hg, primarily in aquatic systems, which is
105 the principal cause of a severe neurological syndrome known as “Minamata Disease”. In order to
106 reduce the amount of Hg released to the environment and limit its exposure to humans, an
107 international treaty, the Minamata Convention on Mercury, was adopted in 2017 (UN, 2017).

108

109 Anthropogenic emissions of Hg to air from global sources stand at an estimated 2220 t y^{-1} in 2015
110 (UNEP, 2018). Canadian anthropogenic Hg emissions were estimated at about 4.3 t y^{-1} (less than
111 0.2% of global anthropogenic emissions) in 2015, with an estimated 58% coming from point
112 sources such as coal-fired power plants and smelters, and 42% from area sources (Zhang et al.,
113 2018; see Figure 1). Anthropogenic Hg emissions in Canada have declined by 85% from 1990 to
114 2010 (from ~ 35 to 5 t y^{-1}), with major reductions from sectors such as the non-ferrous metal
115 mining and smelting (-98%), chemical industries (-95%), waste (-76%), iron and steel industries
116 (-54%) and electric power generation (-30%) (CMSA, 2016). However, due to the steady increase
117 in development of the oil sands, the upstream petroleum sector has shown increases in Hg
118 emissions and accounted for approximately 4.6% of the total Canadian Hg emissions in 2010
119 (CMSA, 2016).

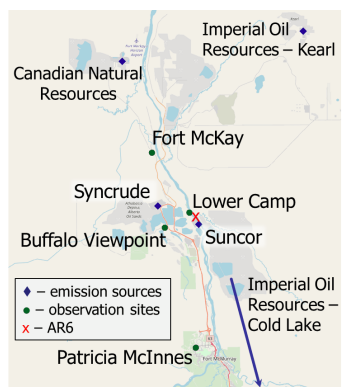


120

121 Figure 1: Spatial distribution of anthropogenic Hg emissions in Canada in 2015 (~ 4.3 t/y). The
122 Athabasca Oil Sands Region is indicated with an approximate rectangular shape within
123 northeastern Alberta, bordering Saskatchewan.

124

125 The Athabasca Oil Sands Region (AOSR) in the northeastern portion of the Canadian province of
126 Alberta (see Figure 1) is a zone of extensive natural resource development. The large natural
127 deposits of bitumen, a heavy crude oil, contained in a mixture of water and clay (called “oil sands”)
128 has led to establishment of large-scale mining and upgrading activities in the area north of Fort
129 McMurray, Alberta (AB) (see map Figure 2). Surface mining and in-situ recovery methods are
130 used to extract bitumen and then upgrade it to synthetic crude oil (Alexander and Chambers, 2016;
131 Larter and Head, 2014). Point source emissions of organics and heavy metals, including Hg,
132 originate from mining activities and upgrading facilities in the AOSR. The upgraders are operated
133 by the companies Suncor, Syncrude, and Canadian Natural Resources. The upgrading process also
134 includes the removal of impurities consisting of sulfur and nitrogen-containing compounds by
135 catalytic hydrotreatment, with volatile hydrogen sulfide and ammonia as by-products. Trace metals
136 contained in the heavy asphaltene fraction are also removed by either stabilization, rejection, or
137 upgrading of asphaltenes (Jia, 2014). The yearly amounts of total Hg emissions from Athabasca
138 oil sands facilities, for the years 2012 to 2015, were between 69 and 25 kg. These annual emissions
139 exhibited an overall downward trend (for details see Table 1 and Figure 3).



140

141 Figure 2: Map of the AOSR with the main point sources for Hg emissions from oil sands
142 developments, and air observation sites. “AR6” marks the approximate midpoint of operations as
143 defined by Kelly et al. (Kelly et al., 2010).

144

145 In 2010, Kelly et al., reported increased concentrations of 13 different trace metals including Hg
146 in the surface waters of the Athabasca River and its tributaries in the oil sands region (Kelly et al.,
147 2010). Observed concentrations were higher near oil sands operations than away from the potential
148 sources. Comparison of upstream and downstream data showed consistently higher concentrations
149 for downstream sites. A similar set of observations was made for Hg in surface snow samples,
150 more specifically, Hg bound to particulates. Concentrations in accumulated snow collected near
151 oil sands developments in March averaged 861 ng m^{-2} compared to less than 100 ng m^{-2} for
152 background measurements (Kelly et al., 2010). Several oil sands installations were identified as
153 potential sources for the elevated observations of Hg, but no direct link between sources and
154 observations was established. Specifically, upgraders were discussed as a source for high Hg levels
155 in the region. Other potential sources included fly ash, road dust, land clearing and mining
156 operations.

157

158 To address the lack of Hg monitoring and attribution of sources, as concluded by Kelly et al.
159 (2010), several follow-up studies were conducted with the intention to establish a conclusive link
160 between measured pollutant concentrations and potential sources in the AOSR (Kelly et al., 2010;
161 Cooke et al., 2017; Kirk et al., 2014; Emmerton et al., 2018; Lynam et al., 2018; Willis et al., 2019;
162 Willis et al., 2018; Gopalapillai et al., 2019). In addition to water and snow samples, other media
163 have been investigated, such as air, biota and sediments. Cooke et al. (2017) studied lake sediment



164 cores sampled from 20 lakes at various distances from oil sands operations, including two of them
165 in the near vicinity (i.e., within 20 km) of the two major upgrading facilities (Suncor and Syncrude)
166 within the region (or site AR6 as designated by Kelly (2010)) (Cooke et al., 2017). The cores
167 provided trace metal data for approximately the past 100-250 years. The cores showed that Hg
168 concentrations have increased by a factor of 3, reflecting the generally accepted scientific finding
169 that global Hg has increased 3-fold as a result of anthropogenic activities since the industrial
170 revolution. No additional increase of Hg concentrations was detected related to the beginning of
171 oil sands operations in the late 1960s. This contrasts with Kelly et al. (2010) and the follow-up
172 study by Kirk et al. (2014) that showed higher Hg loadings in the accumulated snowpack and
173 surface water sampled closer to the mining and upgrading facilities in the AOSR in early spring
174 (March), mostly consisting of PBM of atmospheric origin. While Hg levels were closely correlated
175 with other trace metal concentrations originating from oil sands activities such as nickel and
176 vanadium, no direct causal link with air emissions of Hg, as reported to the National Pollutant
177 Release Inventory (NPRI), was established. Gopalapillai and coworkers recently reported temporal
178 trends in snowpack loadings of total Hg (THg) and methyl mercury (MeHg) (and 44 other
179 elements) (Gopalapillai et al., 2019). Using a composite of snowpack profile samples collected
180 between 2011 and 2016 and data from previous campaigns, a decrease in THg loadings from an
181 average of 510 ng m⁻³ in 2008 to 175 ng m⁻³ in 2016 was found within 8 km from AR6. However,
182 due to the limited temporal coverage (with measurements for THg starting in 2008), the authors
183 suggested a need for additional studies to understand the impact of Hg in the AOSR.

184

185 A recent study by Emmerton et al. (2018) examined lake water samples and related observed Hg
186 and methyl-Hg concentrations to local geology, watershed conditions, and to oil sands activities,
187 with the latter only contributing an estimated <2% of the overall Hg deposited (Emmerton et al.,
188 2018). Long-range transport and biomass burning (i.e., forest fires) were suggested to be the major
189 sources of Hg (Emmerton et al., 2018). Similarly, in a recent study of wet deposition data by
190 Lynam et al. (2018), very low fluxes of Hg deposition were calculated, though the study sites used
191 (AMS6, the Patricia McInnes observation site shown in Fig. 1) were located further away from
192 emitters. Results suggested that dry deposition could, instead, be a more important pathway of Hg
193 removal in the region (Lynam et al., 2018).

194



195 In an effort to explain the elevated Hg concentrations found in the snowpack and waters near oil
196 sands mining and upgrading activities, tailings ponds were studied as a potential source of Hg
197 emissions related to oil sands activities (Willis et al., 2018). However, the water in these ponds
198 (i.e., the non-recycled portion of process water used to process mined bitumen) were found to be
199 an insignificant source of THg and MeHg.

200

201 The above-mentioned studies illustrate recent progress in the ongoing effort to examine the link
202 between observed concentrations and anthropogenic sources of Hg in the AOSR. However, in
203 addition to local emissions, multiple other sources of mercury emissions impact the region,
204 especially forest fires and worldwide anthropogenic and geogenic (contemporary and legacy)
205 emissions that are atmospherically transported into the region. Owing to the much larger emissions
206 of Hg from worldwide sources, as compared to Canadian sources, and the long lifetime of Hg in
207 air, imported Hg accounts for the majority of the Hg burden in Canada (CMSA, 2016), rendering
208 the assessment of the impacts of domestic Hg emissions challenging using measurements alone.
209 While Cooke et al. (2017) investigated the history of Hg deposition in lake catchments via the
210 study of sediment cores, only two lakes sampled were close enough (within 20 km) to oil sands
211 activities, whereas most sites were 20 to >50 km away from the oil sands facilities.

212

213 After Hg is emitted to air from oil sands mining and upgrading activities, transport, transformation
214 and deposition processes determine the distribution and amounts of Hg deposited to environmental
215 media such as vegetation, soils, and water bodies. 3D process-based predictive atmospheric
216 composition models include process representations (such as atmospheric transport, chemical
217 transformations, aerosol particle formation and growth, and wet and dry deposition of gases and
218 particles) and simulate spatiotemporal distributions of pollutants in air and deposition starting from
219 emissions (anthropogenic and natural) as inputs. These models provide insight into transport and
220 transformation pathways of pollutants and causal links between emissions and concentrations
221 observed in environmental media. Models have been applied to study Hg source attribution on
222 global and regional scales, answering questions such as how much a specific emission source
223 contributes to local and regional air concentrations and deposition, and how does the pollutant
224 burden change as industrial activity and related emissions vary (UNEP, 2008; CMSA, 2016;
225 UNEP, 2018)? Model processes are typically constrained by evaluating simulated pollutant levels



226 using observation data from ground-based monitoring networks and research campaigns.
227 Additionally, aircraft measurement data provide observation data on the vertical scale.

228

229 Wildfires are important sources of Hg in Northwestern Canada and climate change is intensifying
230 their frequency (Fraser et al., 2018). Biomass burning primarily releases legacy Hg previously
231 deposited to foliage and soils (Friedli et al., 2001; De Simone et al., 2015). Using multivariate data
232 analysis, Parsons et al. (2013) determined contribution from local sources (i.e., oil sands activities)
233 to be minimal as compared to total gaseous Hg concentrations in the air in the AOSR; however,
234 the authors noted significant episodes of regional forest fires impacting the observed Hg
235 concentrations in the air during the summer months (Parsons et al., 2013).

236

237 **Objectives**

238 Observations of atmospheric Hg in the AOSR are limited to surface air GEM concentrations and
239 Hg loadings in snow. Summertime wet and dry deposition is not measured. Therefore, measured
240 estimates of annual Hg deposition in AOSR is currently not possible. Furthermore, a quantification
241 of the relative importance of different Hg emission sources responsible for Hg loadings in the
242 AOSR is required to prioritize mitigation actions. The 3D mercury model, Global Environmental
243 Multiscale - Modelling Air quality and CHEMistry – Mercury (GEM-MACH-Hg), was applied to
244 develop a comprehensive understanding of atmospheric Hg and deposition levels and pathways,
245 and the role of emissions from Athabasca oil sands activities (particularly from bitumen upgraders)
246 on the spatiotemporal distribution of Hg deposition in AOSR. This study addresses the following
247 questions:

- 248 1. How do air concentrations and ecosystem loadings of Hg species in AOSR compare to
249 other regions in Canada?
- 250 2. What is the level and geographical extent of the contribution of Athabasca oil sands
251 emissions on Hg in air and deposition?
- 252 3. How does the impact of oil sands development on Hg levels in the region compare with
253 the impacts of two other major sources of Hg in the region, biomass burning and global
254 emissions?
- 255 4. What controls the inter-annual variability in Hg levels in AOSR?

256



257 This is the first study that provides a direct connection between Athabasca oil sands Hg emissions
258 and deposition of Hg in and around the AOSR. A similar approach using the model GEM-MACH-
259 Hg was previously applied to the assessment of Hg source apportionment at national and global
260 scales (CMSA, 2016; AMAP/UNEP, 2013; UNEP, 2018).

261

262 **The model and emission inputs**

263 GEM-MACH-Hg (Dastoor et al., 2015) is the mercury version of Environment and Climate
264 Change Canada's 3D process-based operational air quality forecast model GEM-MACH (Global
265 Environmental Multiscale - Modelling Air quality and Chemistry; Makar et al., 2018; Whaley et
266 al., 2018). GEM-MACH includes emissions of gases and aerosols, and simulates meteorological
267 processes, aerosol microphysics, tropospheric chemistry and pollutant dry and wet removal
268 processes from the atmosphere. In addition, GEM-MACH-Hg includes emissions, chemistry and
269 dry and wet removal processes of three Hg species (GEM, GOM and PBM) (Dastoor and Durnford
270 2014; Dastoor et al., 2008; Durnford et al., 2012; Fraser et al., 2018; Kos et al., 2013; Zhou et al.
271 2021). The recent version of GEM-MACH-Hg, previously applied to the investigation of the
272 importance of biomass burning emissions to the Hg burden in Canada (Fraser et al., 2018) and the
273 role of vegetation Hg uptake (Zhou et al. 2021), was used in this study. Oxidation of GEM and
274 gas-particle partitioning of oxidized Hg species (GOM and PBM) are the main chemical
275 transformation processes, and dry deposition of GEM, GOM and PBM, and wet deposition of
276 GOM and PBM are the major removal pathways of Hg in the model. Since observations of
277 snowpack Hg loadings at the end of the winter season are utilized for model evaluation in this
278 study, a detailed representation of the air-cryosphere Hg exchange and transformation processes
279 is important. GEM-MACH-Hg includes a dynamic multilayer air-snowpack–meltwater Hg
280 parameterization, representing Hg accumulation by precipitation and dry deposition to snowpacks,
281 vertical diffusion and redox reactions in snowpacks, and re-volatilization and meltwater run-off of
282 Hg species (Durnford et al., 2012). Geospatially distributed global, regional and local emissions
283 of Hg species (GEM, GOM and PBM) to air from primary geogenic and anthropogenic sources
284 and re-emissions of previously deposited Hg (legacy Hg) from terrestrial and oceanic surfaces are
285 included in the model.

286



287 Three geographical domains were utilized for the model simulations in this study: global, North
288 America (NA) and AOSR. A geospatial resolution of 10 km was chosen for the NA domain and
289 its boundary conditions were determined by the global simulations conducted at $1^0 \times 1^0$ latitude-
290 longitude resolution. Model simulations for the AOSR were carried out at a finer geospatial
291 resolution of 2.5 km for an extended AOSR domain with the approximate midpoint adjacent to the
292 two largest upgrading facilities (called “AR6”) (Kelly et al., 2010) and extending as far north as
293 Hay River, NT, and as far south as Red Deer, AB; the approximate western and eastern extents of
294 the domain are marked, respectively, by Grande Prairie, AB and Flin Flon, MB.

295

296 Geogenic emissions and re-emissions of legacy Hg in soils and oceans ($\sim 4200 \text{ t y}^{-1}$) emitted as
297 GEM were distributed as described in Durnford et al., (2012). Wildfire biomass burning Hg
298 emissions are represented in the model simulations using the FINN (Fire INventory) fire emissions
299 products (Wiedinmyer and Friedli, 2007; Wiedinmyer et al., 2011) together with vegetation-
300 specific emission factors (EFs) as described in Fraser et al. (2018). FINN estimated biomass
301 burning Hg emissions (emitted as GEM) were $\sim 600 \text{ t y}^{-1}$ globally, and 10.8 (2012), 11.4 (2013),
302 15.5 (2014) and 11.1 (2015) Mg/y in Canada, and 13.4 (2012), 10.5 (2013), 11.4 (2014) and 9.5
303 (2015) Mg/y in the US.

304

305 Contemporary global anthropogenic Hg emissions for 2015 (2224 t y^{-1} ; subdivided into GEM,
306 GOM and PBM) developed by the Arctic Monitoring and Assessment Programme (AMAP)
307 (UNEP, 2018) were incorporated into the model for the global scale simulations. For NA and
308 AOSR domains, GEM-MACH-Hg includes monthly and diurnally varying anthropogenic Hg
309 emissions in Canada developed by Zhang et al. (2018), based on the NPRI (NPRI) database (2013)
310 for the major point sources and the 2010 Air Pollutant Emission Inventory (APEI) for the area
311 sources. Anthropogenic Hg emissions in the United States included in GEM-MACH-Hg were
312 based on the 2011 National Emissions Inventory (NEI) (EPA), described in Zhang et al., (2018).
313 Total anthropogenic emissions of Hg in Canada, the United States and worldwide were 4.3, 47 and
314 2224 t y^{-1} , respectively. The GEM:GOM:PBM ratio in the total anthropogenic Hg emissions was
315 approximately 70%:23%:7%.

316



317 For the oil sands activities related Hg emissions, the model's input consisted only of NPRI-
318 reported air emissions. Possibility of fugitive dust from the disturbed landscape due to oil sands
319 activities as a source of particulate-bound Hg emissions was noted by Kirk et al. (2014). Cooke et
320 al. (2017) were unable to detect Hg from dust emissions in lake sediments. Comparison of modeled
321 and observed Hg levels conducted in this study allowed an assessment of whether NPRI reported
322 oil sands emissions and area sources (APEI) in AOSR capture Hg emissions in the region
323 comprehensively or whether there are other yet undetermined important sources of Hg emissions
324 such as from fugitive dust in the AOSR.

325

326 NPRI is a mandatory reporting tool for a wide range of contaminants, including Hg, as prescribed
327 by the Canadian Environmental Protection Act. Facilities are required to report Hg releases, if total
328 work hours exceed 20, 000 and if a reporting threshold of 5 kg y⁻¹ is met for Hg and Hg containing
329 compounds that were manufactured, processed or otherwise used (includes by-products) or
330 contained in tailings and waste rock. For the AOSR domain, Hg emissions were updated in the
331 model from 2012 to 2015 using the NPRI point source Hg emissions data for each year. A summary
332 of Hg emissions from Athabasca oil sands upgrading facilities (NPRI) for 2012-2015 and temporal
333 trend from 2004-2017 are available in Table 1 and Figure 3, respectively. Based on NPRI, total
334 anthropogenic Hg emissions in Canada from the province of Alberta were 605 kg in 2015. Among
335 these, fossil fuel burning activities such as coal-fired power plants, waste incineration facilities
336 and other fossil fuel combustion contributed an estimated 221, 120 and 72 kg, respectively, which
337 represents 68% and, therefore, the bulk of total anthropogenic Hg emissions in Alberta. Iron and
338 steel production together with the cement industry (emitting 55 and 46 kg, respectively) contribute
339 another 14% and oil sands upgrading was a minor contributor (~ 25 kg) in 2015.

340

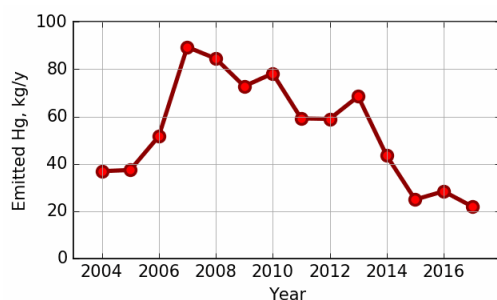
Facility	Latitude	Longitude	2012	2013	2014	2015
Suncor Energy	57.0033	111.466	35	37	0.439	-
Syncrude - Mildred Lake	57.0405	111.619	17	23	30	9.9
Imperial Oil Resources - Cold Lake	54.597	110.399	7	7.4	8.8	11
Imperial Oil Resources - Kearl	57.3969	111.071	-	1.1	4.3	4



	Sum of all four sources	59.0	68.5	43.5	24.9
--	--------------------------------	-------------	-------------	-------------	-------------

341 Table 1: Athabasca Oil Sands Hg emissions (all in kg) reported to NPRI by oil sands processing
342 facilities, and used in the model. For the location of facilities in the AOSR see Figure 2.

343



344

345 Figure 3: Time series of total Hg emissions from oil sands processing facilities in the AOSR. Data
346 was compiled from the NPRI database. Numerical values and individual contributions from 2012-
347 2017 are available in Table 1.

348

349 **Model simulations**

350 Base model simulations at the three model simulation domains (i.e., global, NA and AOSR) were
351 performed using all sources of Hg emissions (as described earlier) and meteorological conditions
352 for the respective years from 2010 – 2015 to allow evaluation of modeled air concentrations with
353 measured air concentrations for all available years in the AOSR. Snowpack Hg measurements in
354 the AOSR started in 2012. Thus, the model-measurement comparison of snowpack Hg and the oil
355 sands Hg emissions impact study was conducted for the years 2012-2015.

356

357 Multiple controlled model simulations from 2012-2015 were performed choosing appropriate
358 geographic domains to assess the relative role of Athabasca oil sands Hg emissions on Hg burden
359 in the AOSR. The impact of Athabasca oil sands emissions was assessed by zeroing out emissions
360 of Hg from oil sands facilities in a controlled simulation using the AOSR domain. Contributions
361 of Hg emissions from biomass burning (in North America) and global anthropogenic sources to
362 the AOSR Hg levels were obtained by zeroing out emissions from these sources in controlled
363 simulations on North America and global model domains, respectively. Source apportionment of
364 the anthropogenic Hg deposition from worldwide sources was conducted using a series of global-



365 scale controlled simulations by zeroing out anthropogenic Hg emissions in different source
366 regions. In addition, controlled model simulations were performed to estimate the individual
367 influences of meteorology, biomass burning emissions and oil sands emissions on the interannual
368 variations in Hg deposition in the AOSR by successively adding these three temporal changes in
369 2013-2015.

370

371 **Mercury observations in the AOSR**

372 Simulated air concentrations and deposition of Hg were evaluated with observations of Hg in air
373 and snowpack in the AOSR. These measurements were recorded with instruments deployed for
374 air quality monitoring purposes and to study the atmospheric deposition of Hg species in the AOSR
375 (Parsons et al., 2013; Kirk et al. 2014; Gopalapillai et al., 2019). Air measurements were carried
376 out at three sites in the AOSR: Patricia-McInnes (2010-2018), Fort Mackay (2014-2018), and
377 Lower Camp (2012-2014). Measurements were made using Tekran 2537 Hg analysers for GEM,
378 and Tekran 1130/1135/2537 systems for speciated Hg (GOM and PBM) fitted with PM_{2.5} and
379 PM₁₀ inlets (see map in Figure 2 for equipment placement and Figure 4-6 for data). Standard
380 operating procedures were provided by the Canadian Atmospheric Mercury Measurement
381 Network (CAMNet, (Steffen and Schroeder, 1999)). Air measurements of oxidized Hg
382 concentrations were carried out at only one site near Fort McKay in 2015 (Parsons et al., 2013).
383 Since Hg deposition to snow is mainly derived from the ambient oxidized Hg concentrations,
384 observations of snowpack Hg loadings provide additional constraint for modeled oxidized Hg
385 concentrations in air.

386

387 Snow samples were collected from 2012 to 2015 at 454 sites located at varying distances from the
388 major upgrading facilities (<1-231 km) to estimate total seasonal Hg loadings in surface snow in
389 the AOSR (Gopalapillai et al., 2019; Kirk et al., 2014). Specifically, 90 (2012), 86 (2013), 140
390 (2014) and 138 (2015) samples were obtained from sites located close to the AOSR emission
391 sources (< 25 km) and at background sites further away from sources (> 120 km). Sample
392 collection was carried out in early to mid-March of each year at approximate maximum snowpack
393 depth based on Environment and Climate Change Canada's National Climate Data and
394 Information Archive historical snow accumulation data (GoC, 2019). Kirk et al. (2014) employed
395 ultra-clean handling and analysis protocols while taking care to avoid local contamination from



396 transportation since sites were accessed by helicopter and snowmobile. Mercury analysis in the
397 snow was carried out using cold vapour atomic fluorescence spectroscopy (Willis et al., 2018; Kirk
398 et al., 2014; EPA, 1996; Bloom and Creclius, 1983). The determined snowpack Hg loading at the
399 end of the winter season represents lower limit of the net wintertime dry and wet deposition of Hg.
400 Hg deposited to snowpacks is partially reduced and re-volatilized to the air and lost during intra-
401 seasonal snowpack melting. Summertime measurements of Hg deposition by scavenging in rain
402 and direct uptake by vegetation, soils and waters were unavailable for model evaluation.

403

404 **Results and Discussion**

405 **Evaluation of model simulated mercury concentrations in air**

406 GEM-MACH-Hg has been extensively evaluated with comprehensive worldwide (including
407 Canada) observations, inter-compared with other Hg models, and applied to mercury assessments
408 in previous studies (Angot et al., 2016; Bieser et al., 2017; Dastoor et al., 2008; Dastoor and
409 Durnford, 2014; Durnford et al., 2010; Durnford et al., 2012; Fraser et al., 2018; Kos et al., 2013;
410 Travnikov et al., 2017; Zhou et al. 2021; AMAP 2013; CMSA, 2016; UNEP, 2018). Model
411 evaluation of ambient Hg in the AOSR is presented in this study. Figures 4-6 provide a comparison
412 of simulated (blue trace) and observed (red trace) daily averaged TGM concentrations in air at the
413 three observation sites (Figure 4: Patricia McInnis, 2010-2015; Figure 5: Lower Camp, 2012-2014;
414 and Figure 6: Fort McKay, 2014-2015), and how the model captured biomass burning events
415 (BBE) (green traces show modeled biomass burning contributions to TGM concentrations). While
416 some observations are incomplete (e.g., June 2013, Patricia McInnis), the data provide a detailed
417 picture of TGM surface concentrations near oil sands activities (see Figure 2 for details). In
418 general, data from all three observation sites and model simulation results agreed well with an
419 average squared Pearson correlation coefficient of 0.6, and measured and modeled median TGM
420 concentrations (\pm standard deviation) of 1.34 ± 0.21 and 1.39 ± 0.17 ng m^{-3} (2011-2015) at Patricia
421 McInnis, 1.36 ± 0.17 and 1.36 ± 0.18 ng m^{-3} (2013) at Lower Camp and 1.22 ± 0.23 and 1.33 ± 0.19
422 ng m^{-3} (2014-2015) at Fort McKay, respectively. The model captured the observed seasonal cycle
423 (typical in the northern hemisphere) with spring maxima and fall minima, shaped mainly by
424 surface fluxes of Hg such as the dominance of re-emission fluxes of Hg from snow in winter and
425 spring and uptake of Hg by vegetation in summer and fall. Transport of Hg from biomass burning
426 (i.e., wildfires) events in northern and western Canada yielded distinct Hg concentration peaks in



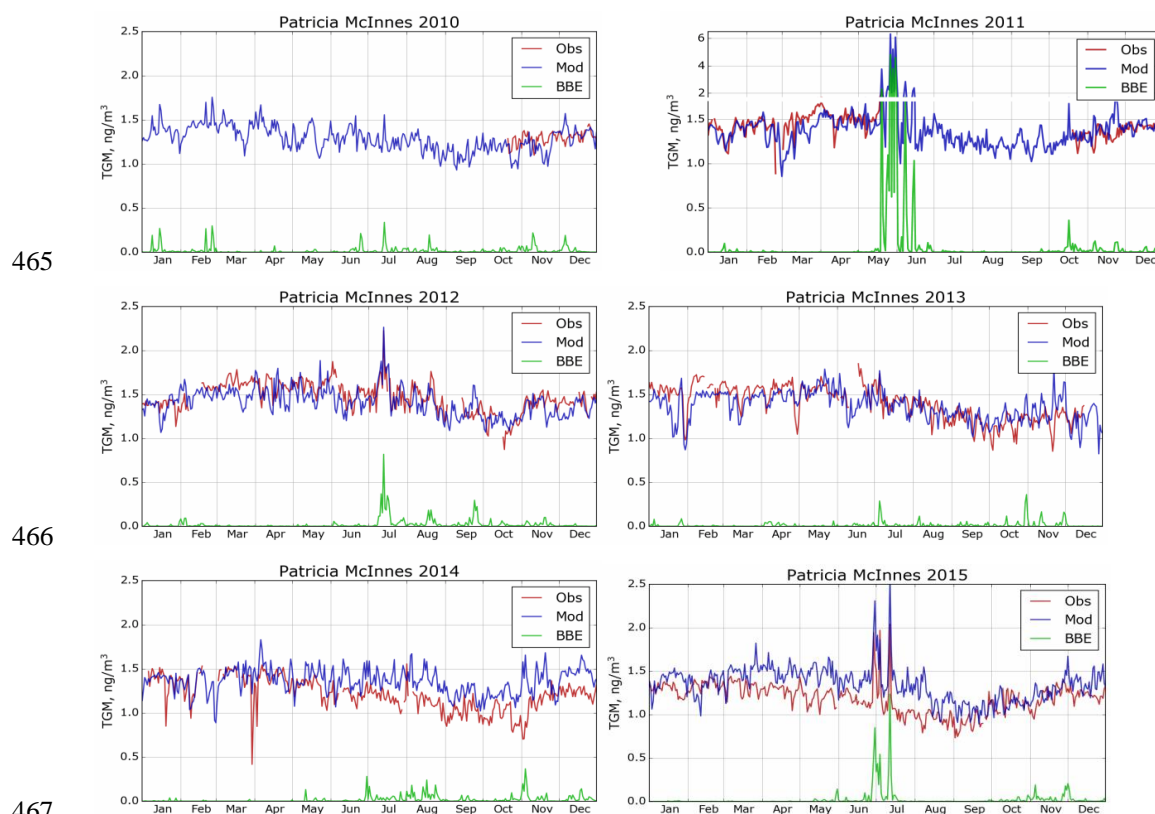
427 TGM concentrations in the AOSR (Figures 4–6). For 2011, biomass burning provided a large
428 contribution to overall TGM concentrations, which peaked during these events at Patricia McInnis;
429 however, no concurrent observations were available for the months of May and June. During the
430 large wildfire events in 2012 and 2015 (June–July), daily averaged TGM concentrations were
431 generally $< 2.5 \text{ ng m}^{-3}$, which were accurately reproduced by the model. However, as shown in
432 Figure 5 for the Lower Camp site in August 2013, there are discrepancies between modeled and
433 observed wildfire events. The impacts of biomass burning emissions on Hg burden in Canada and
434 the uncertainties in wildfire Hg emissions associated with the characterization of wildfire events
435 and emission levels using satellite and field data were described in a previous study (Fraser et al.,
436 2018). Low TGM concentration events in winter and early spring, such as those in March 2014 at
437 Patricia McInnis, were typically associated with clean air masses coming from the Arctic in AOSR.
438 Model-measurement agreement of TGM levels in the air is within the respective model and
439 measurement uncertainties and indicates that reported Hg emissions from AOSR facilities are
440 reasonable.

441

442 GOM and PBM observations were conducted at Fort McKay (a region dominated by natural boreal
443 forest) using $\text{PM}_{2.5}$ (captures particle sizes $< 2.5 \mu\text{m}$) and PM_{10} (captures particle sizes $< 10.0 \mu\text{m}$)
444 inlets in AOSR for 2015, but significant measurement data gaps were present particularly in winter
445 and spring. Observed annual average concentrations were 1.02 ± 2.59 (GOM) and $3.47 \pm 4.79 \text{ pg}$
446 m^{-3} (PBM) using the $\text{PM}_{2.5}$ inlet, and 0.60 ± 1.11 (GOM) and $4.25 \pm 8.23 \text{ pg m}^{-3}$ (PBM) using the
447 PM_{10} inlet in 2015; these observations suggest a dominance of PBM in fine particles ($< 2.5 \mu\text{m}$)
448 at the Fort McKay site (17 km Northwest of AR6). The model simulated and observed average
449 TOM air concentrations and standard deviation ($\pm 1\sigma$) in 2015 were $4.74 \pm 5.06 \text{ pg m}^{-3}$ and $5.74 \pm$
450 7.20 pg m^{-3} , respectively; observed data from both inlets was combined to reduce measurement
451 gaps. Episodes of high concentrations of particulate Hg (up to 72.9 pg m^{-3}), occurring
452 predominantly on coarse ($> 2.5 \mu\text{m}$) particles, that were absent in the modeled PBM
453 concentrations were observed in March. The sources of coarse particles in the AOSR are currently
454 unknown, but fugitive dust from pet coke piles and roads as a result of oil sands mining activities
455 was suggested by Gopalapillai et al. 2019. It should be noted that uncertainty of a factor of 2 or
456 higher with oxidized Hg measurements has been reported (Kos et al., 2013; Gustin et al. 2015).
457 Comparable average GOM and PBM concentrations of 1.89 ± 8.31 and $3.82 \pm 4.90 \text{ pg m}^{-3}$ (mean



458 $\pm 1\sigma$, 2009–2011), respectively, have been measured at a site 8 km from a coal-fired power plant
459 in Genesee, AB (about 500 km southwest of Fort McMurray). Seasonal cycles at the two sites
460 (Fort McKay and Genesee) were similar, with TOM maxima in May–June. Since Hg deposition to
461 snow is primarily driven by the uptake of ambient oxidized Hg species in snowfall and snowpack,
462 the robustness of model simulated oxidized Hg in air was further tested by comparing modeled
463 snowpack Hg loadings with measurements (see next section).
464

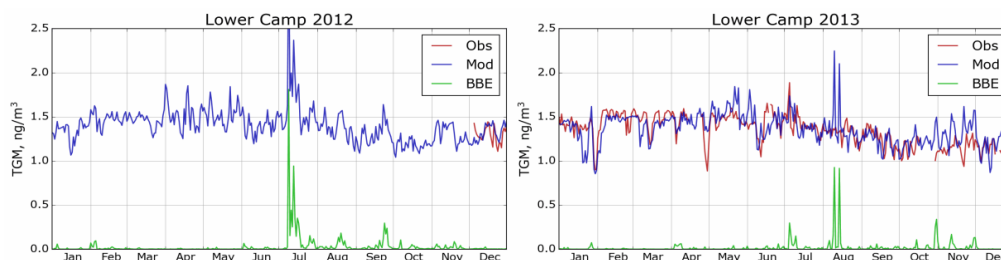


465
466
467
468 Figure 4: Simulated and observed daily averaged surface air TGM concentrations in AOSR for the
469 site Patricia-McInnes (2010–2015). Obs – observations; Mod – model estimation; BBE –
470 modeled biomass burning contributions. Note the larger range of the y-axis to plot the strong
471 biomass burning event in May and June of 2011.

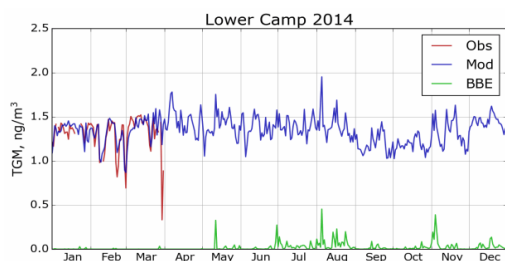
472



473



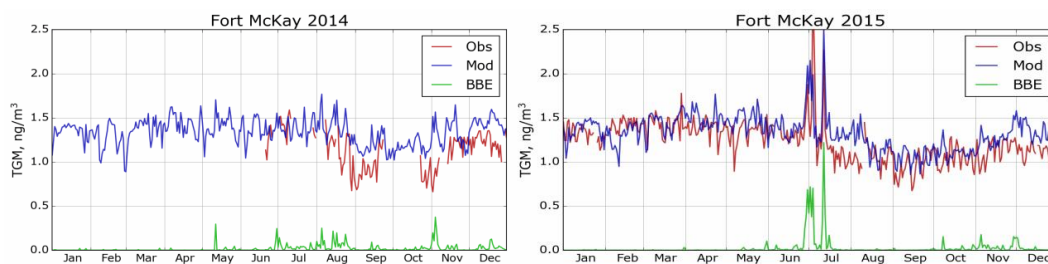
474



475 Figure 5: Simulated and observed surface air TGM concentrations in AOSR for the site Lower
476 Camp (2012—2014). Obs – observations; Mod – model estimation; BBE – modeled biomass
477 burning contribution.

478

479



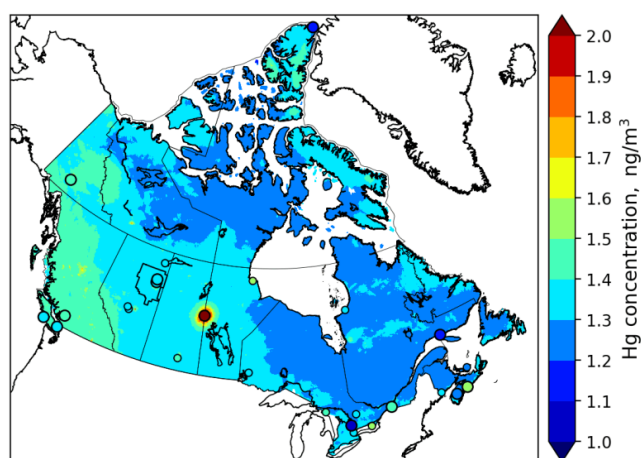
480 Figure 6: Simulated and observed surface air TGM concentrations in AOSR for the site Fort
481 McKay (2014 and 2015). Obs – observations; Mod – model estimation; BBE – modeled biomass
482 burning contributions.

483

484 For the purpose of comparing ambient GEM concentrations in the AOSR with other Canadian
485 regions, Figure 7 provides a map of modeled annual average surface air Hg concentrations of GEM
486 for Canada in 2013. In general, model estimated surface air GEM concentrations agreed well with
487 available observations (in circles), including western Canada, the Pacific coast, and the AOSR.
488 There is a general gradient in GEM concentrations from higher concentrations in the west (1.5 ng
489 m^{-3}) to lower concentrations in the east (1.3 ng m^{-3}). The average air concentrations of GEM in



490 the AOSR (1.40 ng m^{-3} , 2012-2015) reflected the background GEM levels in Canada. The
491 simulated large-scale pattern in GEM concentrations is consistent with, and reflects, a dominant
492 role of trans-Pacific transport of GEM from East Asian Hg sources into Canada and the high
493 Arctic. GEM concentrations are slightly higher in major urban centres and regions of current and
494 past anthropogenic activities such as energy production from coal-fired power plants and mining.
495 The hotspot in Figure 7 near the Saskatchewan/Manitoba border is the former copper-zinc smelter
496 near Flin-Flon, MB, which ceased operations in 2010 (Ma et al., 2012). The soils in the
497 surrounding region remain heavily contaminated with Hg. The re-emission of accumulated legacy
498 mercury in soils (Eckley et al., 2013) is responsible for the highly elevated GEM concentrations
499 in air..



500
501 Figure 7: Model simulated spatial distribution of annual average surface air GEM concentrations
502 in Canada in 2013; colors in circles show observed concentrations for 2013 (large circles) and
503 previous years (small circles).

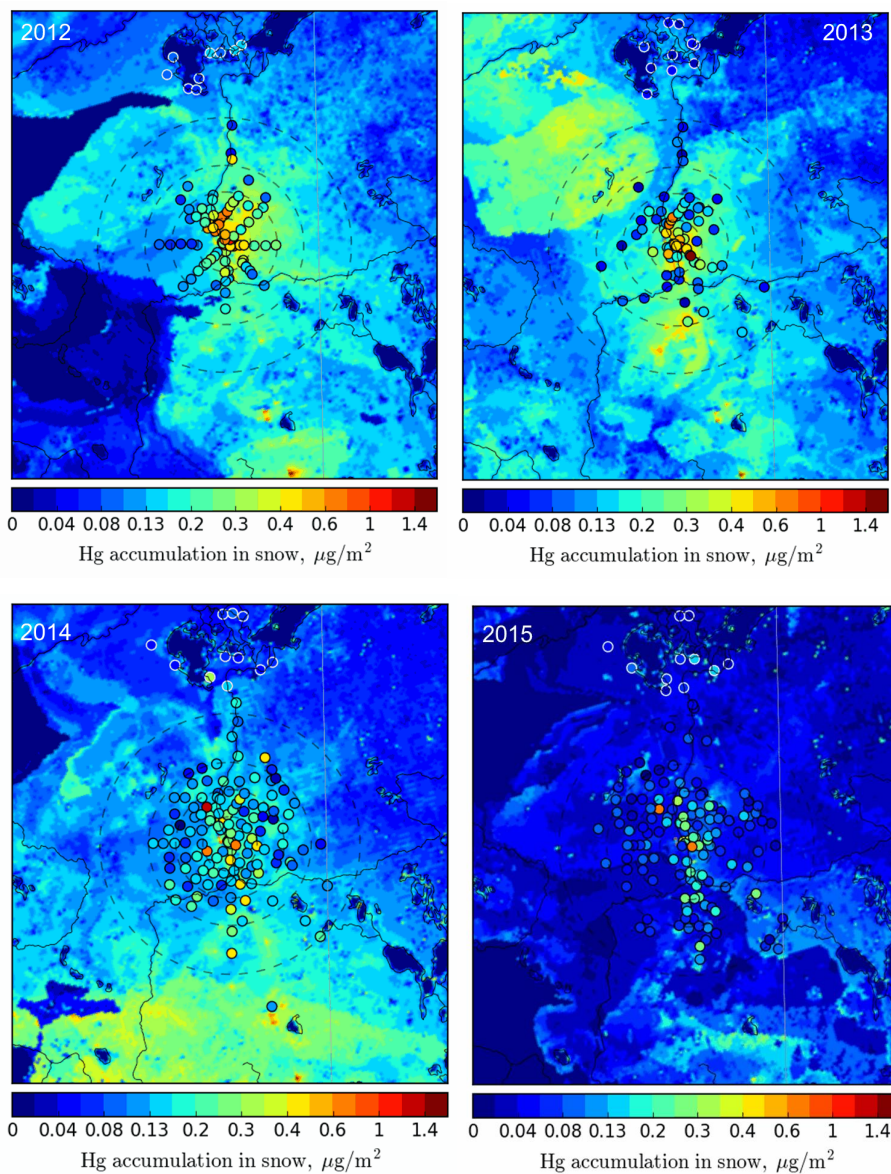
504

505 **Evaluation of model simulated mercury accumulation in snow**

506 Figure 8 compares total Hg loadings in snow simulated by the model with observations (in circles)
507 at the end of winter for years 2012-2015 in the AOSR. Cooke et al., (2017) used dated lake
508 sediment cores to reconstruct deposition trends and anthropogenic enrichment in the region, but
509 several correction factors needed to be applied to estimate Hg deposition fluxes and only two lakes
510 were cored in the direct vicinity of oil sands operations. By comparison, seasonal snowpack Hg
511 data provide the distribution of net total Hg deposition in the region with a large number of



512 sampling sites a short distance (< 25 km) away from sources. However, it should be noted that Hg
513 deposition in the snow is partially reduced and reemitted as well as adsorbed in surface soils due
514 to diffusion and intra-seasonal melt; therefore, snowpack Hg represents the lower limit of net
515 wintertime deposition. Observations at the sampling sites close to sources had the highest
516 snowpack Hg loadings with decreasing concentrations as one moves further away from the
517 immediate source region; the same spatial pattern was predicted by the model, and is most evident
518 for the years with the largest emissions (2012 and 2013; Figure 8). Snow Hg contents at the
519 background sites in the Peace Athabasca Delta region in the north were significantly lower, which
520 was also well reproduced by the model. The figure shows high spatiotemporal variability in snow
521 Hg loadings, which are related to changes in meteorological factors as well as oil sands emissions
522 (as discussed later). The decline in both snowfall amounts and oil sands emissions led to lower
523 snow Hg loadings in 2014 and 2015. Figure 9 shows the model simulated average snow depths in
524 the AOSR and the observed depths at the Mildred Lake site close to the Syncrude upgrader. The
525 model simulates snow amounts and interannual variations accurately. The model-estimated
526 seasonal snow accumulations were 62, 183, 104 and 71 cm between October to May in 2012, 2013,
527 2014 and 2015, respectively. An intense intra-seasonal melting event at the end of February was
528 predicted by the model in each year, which is inline with observations. The largest melting event
529 occurred in 2015, which caused over half of the snow accumulation to melt, and, thus, loss of half
530 of seasonal snowpack Hg loadings. Modeled snow Hg loadings are in agreement with Gopalapillai
531 et al. (2019), who reported a temporal decrease in snow Hg loadings near-field (< 8 km from AR6),
532 from an average load of 510 ng/m² in 2008 to 175 ng/m² in 2016. Relative importance of inter-
533 annual changes in meteorological conditions and oil sands emissions to wintertime Hg deposition
534 is discussed a later section.
535

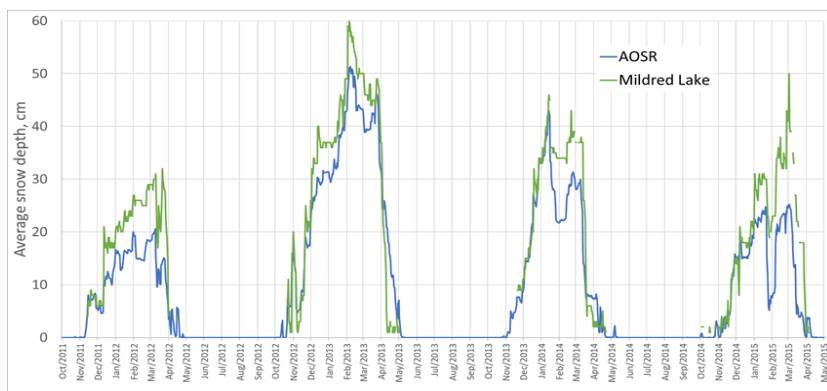


536

537

538 Figure 8: Seasonally accumulated Hg loadings in snow in AOSR from 2012 to 2015: modeled
539 (background map) and observed values (colors in circles). Circles radii: 25, 50, 75, 120 km.

540



541
542 Figure 9: Daily averaged model simulated (blue) and observed snow depths (green) (cm) in 2012-
543 2015 in the AOSR. Modeled values are averaged over the entire AOSR domain and the observation
544 site is Mildred Lake, Alberta, a few km east of the Syncrude oil sands upgrader.

545
546 Figure 10 compares average modeled and observed snow Hg loadings at the sampling locations
547 within 25 km, 25-50 km, 50-75 km, 75-120 and > 120 km distances from AR6. Inter-annual
548 changes in meteorology and oil sands emissions led to decreases in total Hg loads from 0.52 ± 0.21
549 to $0.22 \pm 0.09 \mu\text{g m}^{-2}$ within 25 km of AR6 (from 2012 to 2015) in the snowpack for observation
550 and from 0.39 ± 0.21 to $0.08 \pm 0.06 \mu\text{g m}^{-2}$ for model estimates sampled at sites. The snow Hg
551 loadings of up to $0.7 \mu\text{g m}^{-2}$ were simulated by the model in the immediate vicinity of Hg emitting
552 sources for 2012 (Figure 8). Emitted amounts of Hg from oil sands facilities were reported to the
553 NPRI with the caveat that not all emissions, e.g., emissions of mercury that are part of fugitive
554 dust releases, are captured by the inventory. Brief episodes of Hg on larger particles ($2.5\text{-}10 \mu\text{m}$
555 size) were observed at Fort McKay in late winter, likely originating from fugitive dust in the
556 AOSR. These possible sources of Hg emissions and related deposition (in the vicinity of sources)
557 were not included in the model. At > 120 km from AR6, snowpack loadings were very low for all
558 years at $< 0.1 \mu\text{g m}^{-2}$ with small inter-annual variability, and indicate background Hg
559 concentrations at this distance.

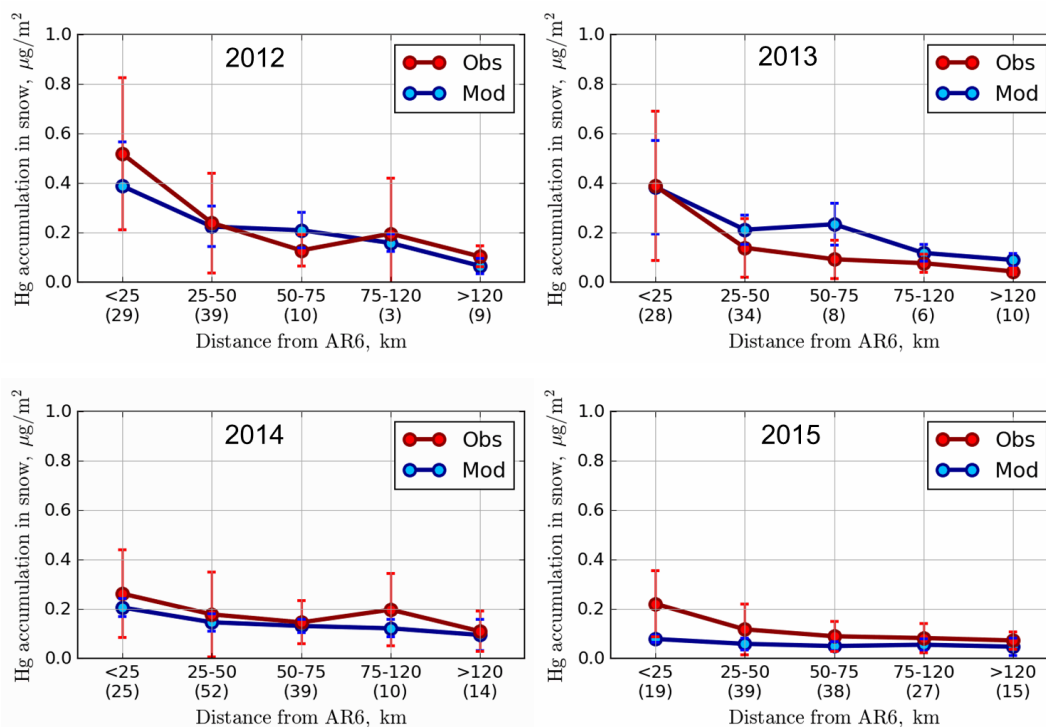
560
561 While the strong decrease away from the source is mirrored in Figure 10 for the years 2012 and
562 2013 (dropping from about $0.4 \mu\text{g m}^{-2}$ at sites located <25 km from AR6 to $< 0.1 \mu\text{g m}^{-2}$ at sites >
563 120 km away), the weaker signature from Figure 8 for the years 2014 and 2015 is more clearly
564 represented in Figure 10, consistent with declines in reported oil sands emissions (see Table 1 and



565 Figure 3). Modeled snow Hg loadings closer to the oil sands sources were lower compared to
566 observed values in 2015. A sensitivity model simulation was conducted for 2015 by replacing
567 NPRI reported Hg emissions from oil sands facilities in 2015 with 2014 values. The sensitivity
568 model simulation matched the observed Hg loadings in the snow in 2015 at all distances; these
569 results suggest that either NPRI Hg emissions from oil sands facilities were slightly under-
570 represented or there was an unaccounted area source (such as from fugitive dust) of Hg in 2015.

571

572 Model estimates and observations agreed well for all distances evaluated, and demonstrate the
573 model's ability in correctly simulating the impacts of changes in Hg emissions and
574 physicochemical processes in the cryosphere. The high variability in the observed snowpack data
575 within 50 km of AR6 indicates that there are likely other local sources around mining facilities
576 that impact local deposition (such as fugitive dust from coke pile and roads). However, modeled
577 estimates at sampling locations agreed with observed snow Hg loadings within one standard
578 deviation, and suggest that unaccounted sources of Hg do not have a significant impact on
579 deposition in the AOSR, likely due to their episodic nature as suggested by observed ambient
580 concentrations of particle-bound mercury.



581

582

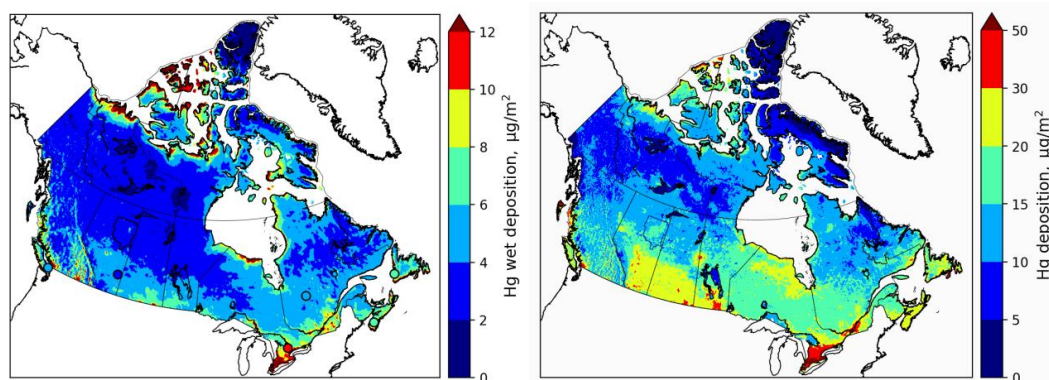
583 Figure 10: Average modeled ($\mu\text{g m}^{-2}$; blue) and observed ($\mu\text{g m}^{-2}$; red) end of winter Hg loadings
584 in snowpack within 25 km, 25-50 km, 50-75 km and 75-120 and > 120 km distances from AR6
585 along with \pm one standard deviations. Modeled accumulated Hg in the snow was sampled at the
586 observation sites. Numbers in parentheses provide number of observation sampling sites in each
587 distance cluster.

588

589 Comparison of modeled annual wet and total deposition (wet plus dry deposition) fluxes of Hg in
590 the AOSR with other locations in Canada is presented in Figure 11 for 2013. In general, spatial
591 distributions of wet and total deposition fluxes followed patterns of precipitation (high in the east,
592 south and mountainous regions of Canada), industrial activities (high in southern Canada),
593 vegetation density (boreal and temperate forests) as well as Hg transport from the US (higher in
594 the east). Figure 11 shows good agreement with observed wet deposition fluxes (noted in circles)
595 in coastal (Saturna Island, BC), rural (Southern Alberta) and urban areas (Egbert, ON). While
596 direct measurements of annual total deposition fluxes are not available, the distribution of Hg
597 deposition fluxes in Canada was found to be consistent with Canada-wide lake sediment inferred



598 deposition fluxes (Muir et al. 2009). Average annual total deposition fluxes in the AOSR were
599 16.9, 15.7, 18.3 and 17.5 $\mu\text{g m}^{-2}$ in 2012, 2013, 2014 and 2015, respectively, slightly higher than
600 in the other regions of northern Alberta ($\sim 14 \mu\text{g m}^{-2}/\text{y}$) and lower than average Hg deposition flux
601 in southern Alberta ($\sim 25 \mu\text{g m}^{-2}/\text{y}$). The highest deposition up to $80 \mu\text{g m}^{-2}$ occurred in southern
602 Ontario in Canada due to the presence of local anthropogenic mercury emissions in these regions.
603



604
605 Figure 11: Model simulated and observed annual Hg wet deposition for 2013 (left) (colors in
606 circles show observed wet deposition for 2013) and simulated annual total Hg deposition (right)
607 (wet plus dry deposition) in Canada for 2013.

608

609 **Impacts of oil sands developments and wildfires on mercury levels in air and deposition**

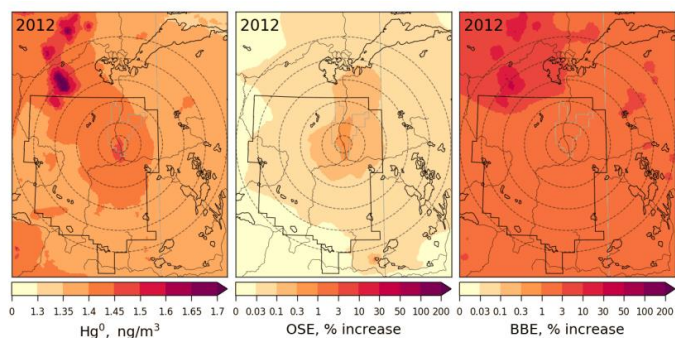
610 Employing GEM-MACH-Hg, the impacts of Hg emissions from oil sands developments in the
611 AOSR on surface air concentrations of Hg species (i.e., GEM and TOM), snowpack Hg loadings,
612 and annual Hg deposition were investigated for the years 2012-2015. Since Northwest Canada is
613 a region of high wildfire activity (Fraser et al. 2018), the relative role of Hg emissions from
614 biomass burning in North America on the Hg burden in the AOSR was also examined.

615 Figures 12 & 13 provide spatial distributions of simulated annual average surface air
616 concentrations of GEM (globally transported and the dominant ambient Hg species) and TOM
617 (regionally transported and efficiently deposited Hg species) (left panels) for the years 2012 to
618 2015 along with their contributions (as % increases) from oils sands emissions (OSE, middle
619 panels) and biomass burning emissions (BBE, right panels) in the AOSR and the surrounding
620 region. GEM air concentrations were 1.4 ng m^{-3} in the AOSR in 2012-2015, which is within the

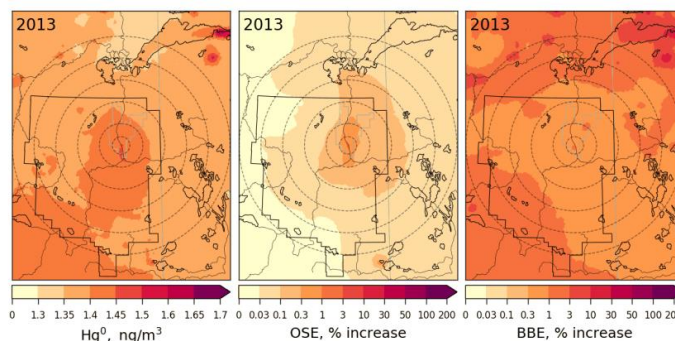


621 range of GEM concentrations observed in Alberta (i.e., 1.2-1.5 ng m⁻³ in 2012). While annual
622 average GEM concentrations were slightly elevated close to the major upgraders (> 1.5 within 5
623 km vs 1.4 ng m⁻³ 200 km away from AR6) in the AOSR, GEM concentrations were found to be
624 elevated up to 1.8 ng m⁻³ in surrounding regions of the AOSR due to local wildfires in 2012-2015.
625 Since the lifetime of GEM in the air is between 0.5-1 year, GEM concentrations are largely driven
626 by global transport in the AOSR (and Canada) with only minor contributions from local emissions.
627 Oil sands emissions increased atmospheric GEM concentrations up to 2.3% in 2012 and 2013, and
628 negligibly (up to 0.9%) in low OSE years 2014-2015, only very close to the upgraders (i.e., within
629 2.5 km). Wildfire activities are highly variable from year to year, and can significantly impact
630 GEM concentrations in the AOSR in summertime (Fraser et al. 2018). Biomass burning
631 contributed to 1.0-2.2% increases in average GEM concentrations in and around the AOSR (Figure
632 12, right panels), making biomass burning a more important source of GEM than OSE in the
633 region. Strong regional biomass burning events led to large increases in GEM concentrations of
634 up to 35% (2012-2015) in the AOSR and the surrounding regions.

635

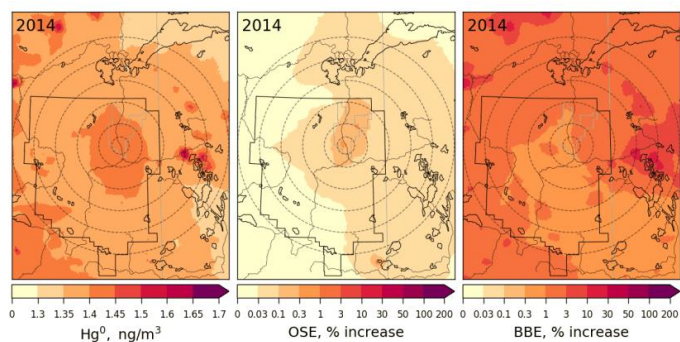


636

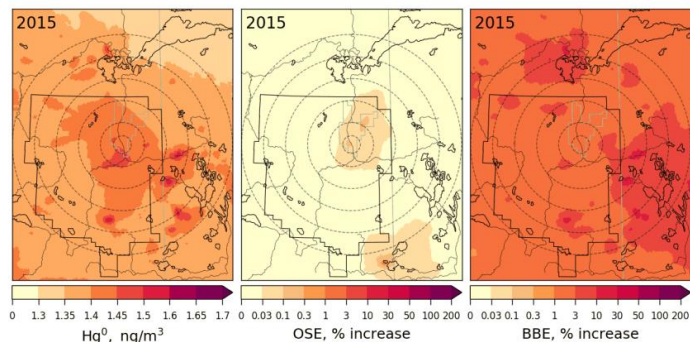




637



638



639 Figure 12: Annual average surface air concentration of GEM (left) and concentration enrichments
640 (%) due to Hg emissions from Athabasca oil sands operations (OSE, middle) and biomass burning
641 in North America (BBE, right) for the years 2012 to 2015. The AOSR is marked as an approximate
642 rectangle, and concentric distance circles are at 20, 50, 100, 150, 200 and 250 km from AR6.

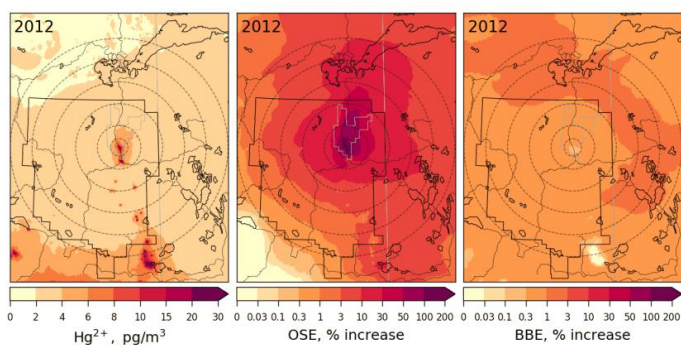
643

644 While average surface air TOM concentrations in the AOSR were only 3.3 pg m^{-3} (consistent with
645 observations), hot spots were modelled in the immediate vicinity of the major upgraders ($> 25 \text{ pg}$
646 m^{-3} within 5 km from AR6 in 2012-2013) in the AOSR (Figure 13, left panels). In 2014-2015,
647 TOM concentrations around AR6 were about half of 2012-2013 (12 pg m^{-3}), consistent with
648 reported changes in Hg emissions from the respective facilities. OSE are found to be the main and
649 a major contributor of oxidized Hg concentrations in surface air close to oil sands sources,
650 increasing background concentrations over 30% within 100 km and 60% within 50 km from AR6
651 in 2012-2013, particularly in the northeast sector of the AOSR. Wildfire emissions played a minor
652 role in ambient TOM concentrations in the region, contributing to $< 1\%$ increases in 2012, 2013
653 and 2015, but increased to $\sim 6\%$ in 2014 as a result of higher wildfire activities. Hg emitted from

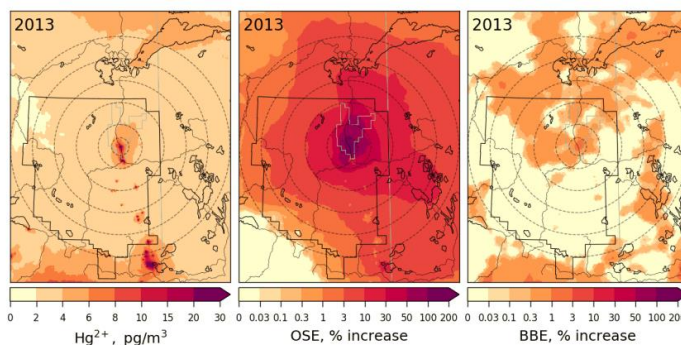


654 oil sands operations as oxidized species is deposited efficiently by precipitation and uptake from
655 terrestrial surfaces in the vicinity of the sources. By comparison, most of the GEM emissions are
656 transported out of the region except for a small fraction being deposited locally via direct
657 vegetation uptake and conversion to oxidized species and dry deposition. Oxidized Hg species
658 emitted from global sources do not reach the AOSR via long-range transport due to their short-
659 lived nature. As a result, OSE-related Hg deposition in the AOSR consists primarily of TOM,
660 whereas, long-range transport of GEM accounts for the deposition in the AOSR attributed to
661 outside sources. Wildfire emissions are mostly assumed to be emitted as GEM as indicated by
662 observations (Friedli et al. 2001).
663

664

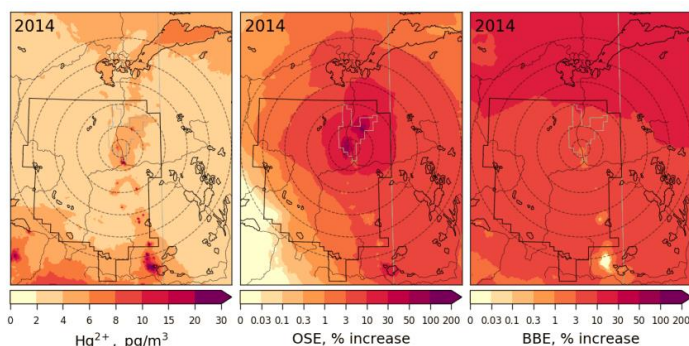


665

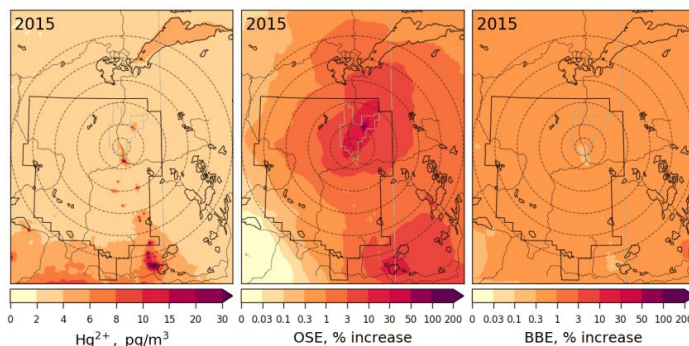




666



667



668 Figure 13: Annual average surface air concentration of TOM (sum of GOM and PBM, left), and
669 concentration enrichments (%) due to Hg emissions from Athabasca oil sands operation (OSE,
670 middle) and biomass burning in North America (BBE, right) for the years 2012-2015. AOSR is
671 marked as an approximate rectangle and concentric distance circles are at 20, 50, 100, 150, 200
672 and 250 km from AR6.

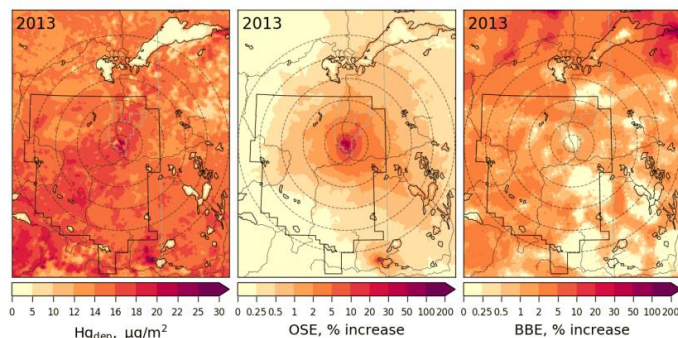
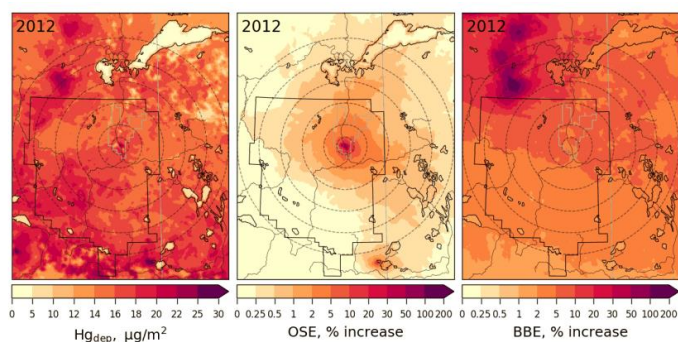
673

674 Figures 14 and 15 provide spatial distributions of modelled annual total mercury deposition (Figure
675 14, left panels) and seasonally accumulated Hg loadings in the snow (Figure 15, left panels), and
676 their source attributions to OSE (Figure 14, middle panels; Figure 15, right panels) and BBE
677 (Figure 14, right panels) in the AOSR in 2012-2015. Mercury deposition fluxes from 7-28 $\mu\text{g m}^{-2}\text{y}^{-1}$
678 $(15.6 - 18.3 \mu\text{g m}^{-2}\text{y}^{-1}, \text{averages})$ were modelled in the AOSR in 2012-2015, originating from
679 all Hg emission sources - global primary and legacy anthropogenic and geogenic (including oil
680 sands and biomass burning) emissions. Since the contribution of global transport of GEM to the
681 ambient total Hg concentrations in the AOSR is much larger than the contributions of OSE and
682 BBE (Figure 12) and GEM concentrations are typically 2-3 order of magnitude higher than TOM

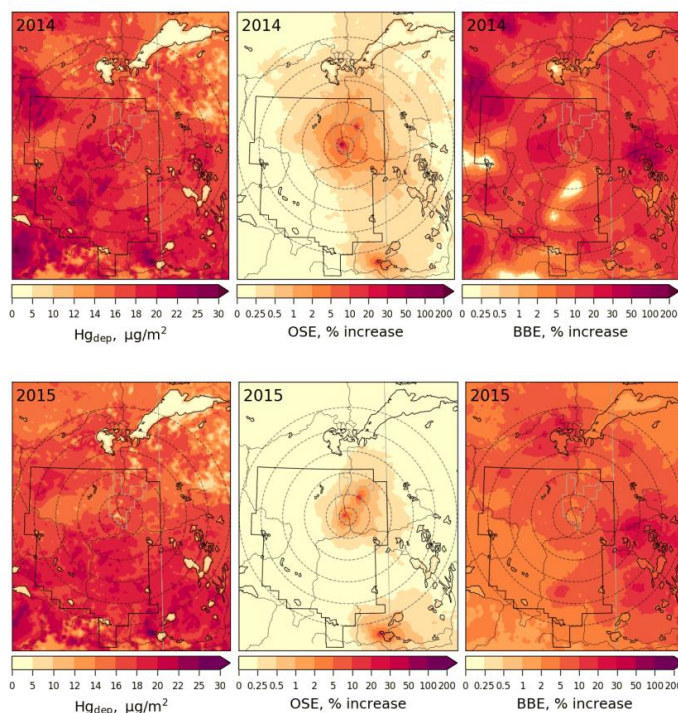


683 concentrations (which have higher contributions from OSE, Figure 13), deposition of imported
684 GEM makes up a major portion of the annual Hg deposition in the AOSR on a broad spatial scale,
685 despite its lower Hg deposition efficiencies than TOM (Figure 14). Similar to ambient TOM
686 concentrations, modelling reveals the impact of OSE to Hg deposition to be greatest in the vicinity
687 of upgraders, i.e., average increases of 17%, 20%, 8%, and 3% within 20 km of AR6 in 2012,
688 2013, 2014 and 2015, respectively, and < 1 % beyond 50 km in all years. Model results reveal a
689 larger impact of OSE on Hg deposition in the regions northeast of oil sands sources, consistent
690 with observations and prevailing wind direction and speed (Kirk et al. 2014). Average Hg
691 deposition contributions due to BBE (increases of 1.4-13%) were higher than OSE contributions
692 (increases of 0.3-1.3%) across 200 km of oil sands operations in 2012-2015. Wildfires in the
693 region led to localized increases in Hg deposition of up to 193% and 101% in 2012 and 2014,
694 especially northwest of the AOSR. Mercury emissions from electricity generation in southern
695 Alberta accounted for a general decrease in Hg deposition fluxes from south to north around the
696 AOSR.
697
698

699



700



701

702

703 Figure 14: Annual total Hg deposition flux (left) and deposition enrichments (%) due to Hg
704 emissions from Athabasca oil sands operations (OSE, middle) and biomass burning in North
705 America (BBE, right) in 2012-2015. The AOSR is marked as an approximate rectangle and
706 concentric distance circles are at 20, 50, 100, 150, 200 and 250 km from AR6.

707

708 Snowpack Hg accumulations from the start of the snow season to the end of winter (roughly
709 coinciding with the maximum snow accumulation period) and their contributions from oil sands
710 Hg emissions were estimated for 2012-2015 (Figure 15). Background snow Hg loadings (without
711 the impact of OSE, middle panels) were spatially highly variable (up to $1.4 \mu\text{g m}^{-2}$) in the region
712 between 2012-2015. The higher snow Hg background levels resulted from both the regional
713 transport of Hg from southern Alberta as well as spatial inhomogeneity in the accumulation of
714 snow. Closer to OSE sources, total Hg loadings in snow reached up to $1.0 \mu\text{g m}^{-2}$ (< 20 km from
715 AR6) in 2012-2014 (Figure 15). In 2015, emissions from oil sands-related activities were the
716 lowest and total Hg loadings corresponded to background emissions. The impact of OSE was
717 notably greater to the snowpack Hg loadings, including the spatial extent, than to the annual Hg



718 deposition (Figure 15, right panels). Average increases of 55%, 43%, 35% and 7% in snow Hg
719 amounts were simulated within 50 km of AR6 in 2012, 2013, 2014 and 2015, respectively, as a
720 result of OSE. Regions northeast of the AOSR showed increases of 27-44% in snow Hg levels in
721 2012 and 2013 and 3-24% in 2014 and 2015 between 50-100 km from AR6. Model results support
722 the conclusions of previous studies that oil sands Hg emissions have a large impact on snow Hg
723 loadings near the oil sands emission sources with decreasing contributions away from AR6 (Kelly
724 et al., 2010; Kirk et al., 2014). The distinctive pattern of higher snow Hg loadings in the northeast
725 region surrounding the AOSR was also reported (Kirk et al., 2014). Model results reveal high
726 spatiotemporal variability in background snow Hg loadings; this is related to variability in snowfall
727 amounts, meteorological conditions affecting melting and snowpack Hg processes including
728 redox, air-snow exchange and transport to soils.

729

730 Average annual Hg deposition fluxes in the AOSR were 13.3 (2015) to 18.5 (2013) $\mu\text{g m}^{-2}\text{y}^{-1}$
731 within 10 km, 15.0 (2015) to 16.9 (2013) $\mu\text{g m}^{-2}\text{y}^{-1}$ between 10-20 km, and $\sim 16 \mu\text{g m}^{-2}\text{y}^{-1}$ 50 km
732 away from the major oil sands emission sources. In the AOSR, winter (and snow cover) can last
733 up to six months (from November to April) with maximum snow depths in January-February.
734 Winter (November-April) and summer (June-August) periods contributed to $\sim 20\%$ and 50% ,
735 respectively, of annual Hg deposition in AOSR. In Figure 16, three representative months in the
736 winter (December to February) and summer (June to August) seasons, each, are chosen to present
737 the inter-seasonal contrast in OSE impacts on Hg deposition along with the impact on annual
738 deposition as a function of distance from AR6.

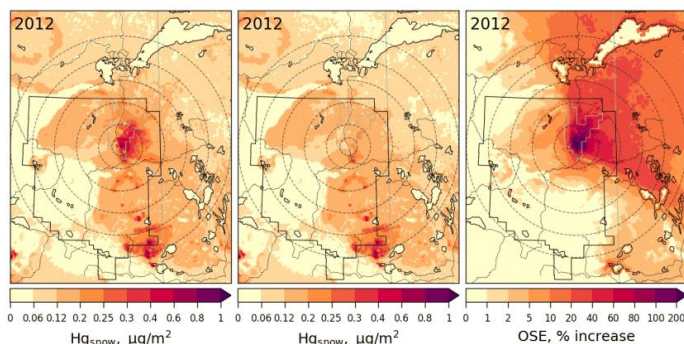
739

740 Seasonally, OSE accounted for the largest Hg deposition increases in winter months: $\sim 230\text{-}500\%$
741 (2013), $146\text{-}374\%$ (2012), $94\text{-}104\%$ (2014) and $40\text{-}43\%$ (2015) within 10 km; 75% (2013), 57%
742 (2012), 25% (2014) and 5% (2015) at 20 km; and $24\text{-}33\%$ (2012-2013) and $6\text{-}12\%$ (2014-2015) at
743 50 km distance from the major oil sands upgraders. In summertime, lower deposition increases
744 due to OSE were estimated, $\sim 13\text{-}56\%$ (2012-2013) and $3\text{-}7\%$ (2014-2015) within 10 km, and $<$
745 7% (2012-2015) at 20 km from AR6. Annually, OSE accounted for deposition increases of $\sim 24\text{-}$
746 70% (2012-2013), 14% (2014) and $< 5\%$ (2015) within 10 km, 10% (2012-2013) and $< 5\%$ (2014-
747 2015) at 20 km, and $< 4\%$ (2012-2015) at 50 km from the major oil sands emission sources. These
748 seasonal variations are consistent with inter-seasonal differences in Hg deposition pathways (i.e.

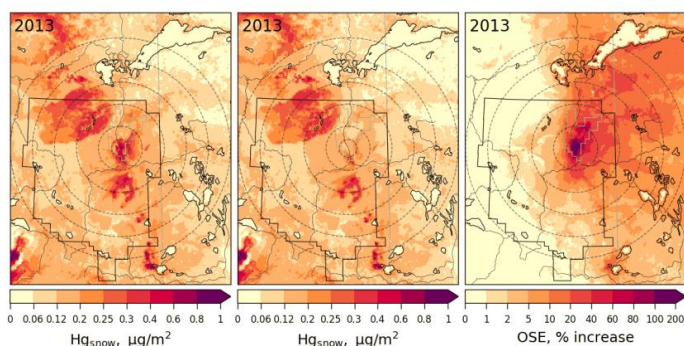


749 the dominant role of GEM uptake by vegetation in summer from global sources, and uptake of
750 local TOM emissions by snowfall and snowpack as the main pathway in wintertime deposition)
751 (Graydon et al., 2006; Obrist et al., 2016; Zhang et al. 2009). The influence of OSE to summertime
752 and annual depositions is also more limited spatially (up to 30 km of OSE) than to wintertime
753 deposition (up to 100 km of OSE), consistent with observations (Kirk et al, 2014; Gopalapillai et
754 al., 2019).
755
756

757

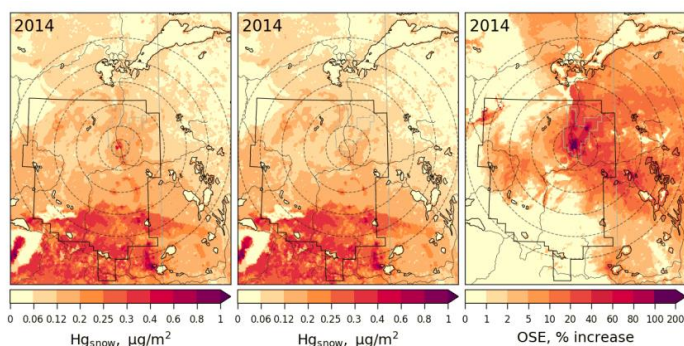


758

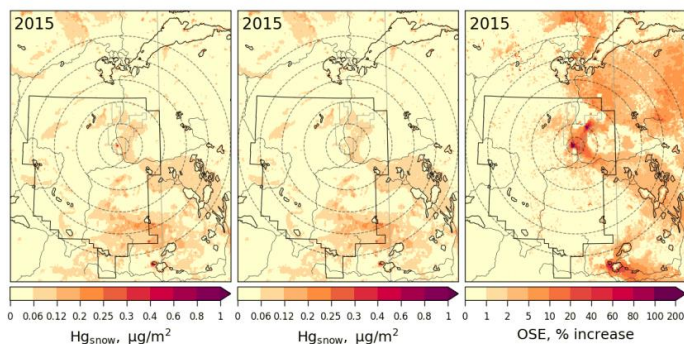




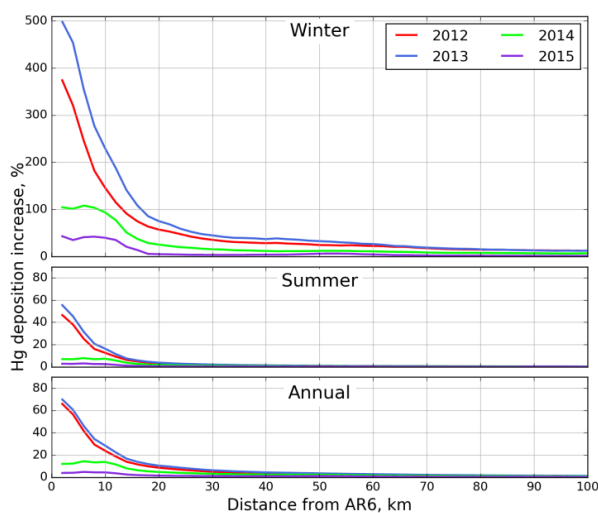
759



760



761 Figure 15: Seasonally accumulated Hg loadings in snow with all Hg emissions (left) and
762 Athabasca oil sands Hg emissions (middle), and enrichments (%) in seasonally accumulated Hg
763 loadings in snow due to Athabasca oil sands Hg emissions (OSE, right) in 2012-2015. The AOSR
764 is marked as an approximate rectangle and concentric distance circles are at 20, 50, 100, 150, 200
765 and 250 km from AR6.
766



767

768 Figure 16: Average Hg deposition enrichments (%) due to Athabasca oil sands emissions in winter
769 from December to February (top), in summer from June to August (middle), and annually (bottom)
770 for 2012 (red), 2013 (blue), 2014 (green) and 2015 (pink) by distance from AR6.

771

772 **Process attribution of interannual variations in mercury deposition**

773 The interannual differences noticed in Figure 16 raises the question of the contributing factors to
774 the interannual variability of Hg deposition in different seasons, especially close to the processing
775 facilities (i.e., within a 10 and 20 km radius). The relative importance of variations in
776 meteorological conditions and changes in OSE and BBE on the temporal changes in Hg deposition
777 fluxes from 2012 to 2015 were analyzed. Since meteorological changes are expected to occur
778 regardless of changes in emissions, a controlled model simulation was first conducted by applying
779 meteorological changes only from 2012 to 2015. Subsequently, two additional model simulations
780 were performed by including changes in BBE and OSE successively. It should be noted that
781 interannual variations in meteorological factors (synoptic as well as local scale) affect overall
782 seasonal and annual deposition rates and, therefore, the magnitude of the impacts of various
783 emissions on the deposition, irrespective of the changes in emissions; thus, the results presented
784 here are cumulative contributions of changes in meteorology and emissions. Figure 17 presents
785 process attribution of interannual changes in winter (top), summer (middle) and annual (bottom)
786 Hg deposition rates from 2012-2015 within 0-10 km (left) and 10-20 km (right) from AR6.. The
787 lower panels illustrate Hg deposition source contributions from global emissions (green; global



788 anthropogenic (except oil sands), geogenic and re-emission), OSE(red) and BBE(purple), and the
789 upper panels show process contributions of changes in meteorology (blue), oil sands (red) and
790 biomass burning (purple) emissions to interannual changes in total Hg deposition.

791

792 While wintertime Hg deposition fluxes were relatively low ($2.6\text{--}3.6\ \mu\text{g m}^{-2}$, November-April; 0.3
793 $\text{--}0.8\ \mu\text{g m}^{-2}$, December-February) in the AOSR, oil sands emissions were a major source of Hg
794 deposition close to the oil sands sources as explained earlier, contributing to 70-80% of deposition
795 within 10 km of AR6 in high oil sands emission years (2012 and 2013). Wintertime (net) Hg
796 deposition to northern landscapes is controlled by cryospheric processes, which exhibit strong
797 interannual variations; therefore, interannual variation in wintertime Hg deposition is strongly
798 controlled by meteorological conditions including snowfall amounts, wind speed, surface air
799 temperature, solar insolation, and intra-seasonal melting affecting air-snow-soils exchange
800 processes of mercury (Faïn et al., 2013). In 2015, a large snowmelt event at the end of February
801 effectively removed about half of the accumulated mercury in snow resulting in much lower snow
802 Hg content at the time of sampling (see Figure 9).

803

804 Surface temperature and intra-seasonal melting have a large impact on how much of the deposited
805 Hg in the snow is re-emitted back to the atmosphere and how much is adsorbed to surface soils,
806 altering snow Hg loadings and net wintertime Hg deposition. Since 2013 experienced deeper
807 snowpack and less inter-seasonal melting, a larger fraction of snowpack Hg was reduced and
808 revolatilized, leading to a lower net Hg deposition despite slightly higher oil sands Hg emissions
809 compared to 2012. Conversely, lower snowpack depth and a strong melting event at the end of
810 February in 2015 allowed a large fraction of snowpack Hg to be transferred and retained in
811 underlying soils increasing net Hg deposition, particularly the background deposition contribution.

812

813 Within 10 km of major oil sands sources, wintertime variations in meteorology led to Hg
814 deposition declines of 17% in 2013 and 2014 and increases of 10% in 2015 along with OSE-led
815 deposition declines of 10% (2013), 35% (2014) and 56% (2015). When combined, the net effect of
816 these two factors were overall reductions in wintertime Hg deposition fluxes of 27% (2013), 52%
817 (2014) and 46% (2015), relative to 2012. At a distance of 10-20 km from the oil sands sources,
818 changes in meteorology led to a 54% increase in wintertime Hg deposition in 2015, but the overall



819 deposition only increased by 19%, because the decline in oil sands Hg emissions reduced the
820 deposition by 35%. River discharge rates and Hg concentrations are reported to be highest in the
821 spring meltwater flood (between 3 ng/L and 16 ng/L, up from typically <2 ng/L at their lowest
822 annual level) in tributaries of the Athabasca River and pose risk to the downstream environments
823 (Kelly et al., 2010; Wasiuta et al., 2019). Since the ground is still frozen at the time of spring
824 freshet, Hg runoff is derived from seasonal snowpack loadings and mobilization of Hg from
825 surface soils, both of which are contaminated by oil sands emissions in proximity of the sources
826 and show a sensitivity to changes in Hg emissions from oil sands developments.

827

828 Compared to winter, AOSR summertime background Hg deposition fluxes were significantly
829 higher (~6.3-7.5 $\mu\text{g m}^{-2}$, 2012-2015) and less variable in space and time, and OSE contributions to
830 total deposition were relatively lower (~ 0.05-0.5 $\mu\text{g m}^{-2}$ within 10 km and 0.01-0.2 $\mu\text{g m}^{-2}$ from
831 10-20 km, 2012-2015). In addition, summertime biomass burning emissions contributed to Hg
832 deposition of 0.1-0.4 $\mu\text{g m}^{-2}$ (2012-2015). Summertime Hg deposition to terrestrial systems is
833 temporally less variable than wintertime deposition as it is predominantly driven by Hg uptake by
834 vegetation and soils followed by wet deposition. Changes in oil sands emissions played a more
835 significant role than the meteorological factors in summertime inter-annual Hg deposition
836 variations.. Compared to 2012, changes in meteorology, biomass burning and oil sand emissions,
837 respectively, led to changes in summertime Hg deposition fluxes by -3%, -2%, and +7% in 2013,
838 +3%, +2% and -15% in 2014, and -1%, +4% and -20% in 2015, resulting in overall changes in Hg
839 deposition by +2% (2013), -10% (2014) and -17% (2015), within 10 km of major oil sands sources.
840 Interannual variations in precipitation amounts and its impact on the wet deposition of Hg was the
841 primary reason for the meteorology-related changes in summertime Hg deposition fluxes.

842

843 Since summertime deposition contributes to about half of the annual deposition, interannual
844 changes and their responsible factors in annual Hg deposition fluxes had a similar pattern as
845 summer, with a relatively larger impact of changes in OSE on Hg deposition fluxes in the
846 immediate vicinity of oil sands sources. Relative to 2012, deposition increases were 6 (2014) and
847 1% (2015) due to variations in meteorology and 2% (2014-2015) due to biomass burning, and
848 deposition declines were 15 (2014) and 23% (2015) due to reduction in oil sands Hg emissions.
849 This results in overall reductions in annual Hg depositions of 7 (2014) and 20% (2015) within 10



850 km of AR6. These model results demonstrate that reduction in Hg emissions from oil sands
851 processing activities lead to measurable declines in mercury deposition fluxes in AOSR. Further
852 away from sources (right panel, Figure 17), the changes in meteorology and oil sands emissions
853 resulted in comparable changes in Hg deposition rates (+9 (2014) and +5 % (2015), meteorology;
854 -4 (2014) and -9% (2015), OSE) along with 3(2014) and 2(2015)% increases in deposition due to
855 BBE, resulting in relatively smaller overall changes (+8% (2014) and -2% (2015)) in Hg deposition
856 fluxes. Interestingly, land clearing in the AOSR contributes to reduced background Hg deposition
857 fluxes due to the reduction in foliage Hg uptake; average background Hg deposition fluxes were
858 about $1 \mu\text{g m}^{-2}$ lower within 10 km as compared to Hg deposition fluxes 20 km away from the
859 major oil sands activities.
860



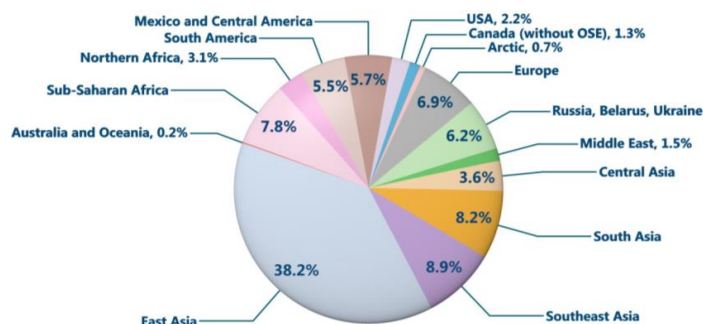
861
862 Figure 17: (a) December – February, (b) June – August and (c) yearly averaged source
863 apportionment of total Hg depositions (lower panels) in 2012-2015, and contributions of changes
864 in meteorology, Athabasca oil sands emissions and biomass burning emissions (only in summer)
865 (top panels) to the changes in total Hg depositions in 2013-2015 relative to 2012, within 10 km
866 (left plot) & 10-20 km (right plot) of AR6.
867



868 **Source apportionment of the background mercury deposition**

869 As noticed in Figure 14-16, background Hg (long-range transport from global source regions;
870 excludes impact of oil sands emissions, but includes impact of all other Hg emissions in Canada)
871 is responsible for the majority of annual Hg deposition in the AOSR (except in winter in the
872 vicinity of major oil sands Hg emission sources). The average annual background Hg deposition
873 in the AOSR was $15.3\text{--}16.7 \mu\text{g m}^{-2}\text{y}^{-1}$ in 2012-2015. This includes ~40% deposition from
874 contemporary global anthropogenic Hg emissions (excluding Hg emissions from Athabasca oils
875 sands activities) and ~60% from global geogenic emissions and re-emissions of legacy mercury
876 deposition (of both anthropogenic and geogenic origin). The model was applied to investigate the
877 relative proportions of background anthropogenic Hg deposition fluxes contributed from various
878 worldwide emission source regions, including Canada, in the AOSR (Figure 18). Almost 50% of
879 the background anthropogenic Hg deposition originated from East and Southeast Asia, a region of
880 high economic activity and high energy demand, which is sourced for the most part by coal-fired
881 power plants. The model estimated that foreign anthropogenic sources accounted for over 98% of
882 the background anthropogenic Hg deposition in the AOSR of which present-day emissions in East
883 Asia, Southeast Asia, South Asia, Sub-Saharan Africa, Europe and the United States contributed
884 to approximately 38%, 9%, 8%, 8%, 7%, and 2%, respectively. Emissions from present-day
885 anthropogenic sources in Canada (excluding oil sands sources in AOSR) contributed to < 2% of
886 the background anthropogenic Hg deposition nationally including the AOSR. In proximity of oil
887 sands activities, oil sand Hg emissions are a significant source of Hg deposition as demonstrated
888 earlier in this study. By comparison, oil sands developments currently have a negligible impact on
889 Hg deposition on a broader spatial scale in Canada. These results highlight the need for worldwide
890 mitigation efforts, in addition to the local efforts, to reduce the risks of mercury contamination in
891 the AOSR.

892



893
894 Figure 18: Deposition contributions from global anthropogenic source regions (excluding
895 Athabasca oil sands Hg emissions) to the average contemporary anthropogenic Hg deposition
896 portion (40% of total deposition) of the total deposition in Athabasca Oil Sands Region in 2015.
897

898 Conclusions

899 An assessment of mercury levels in air and deposition in the Athabasca oil sands region (AOSR)
900 in Northern Alberta, Canada, was conducted to investigate the contribution of Hg emitted from oil
901 sands activities on the surrounding landscape using a 3D process-based Hg model in 2012-2015.
902 The model-simulated Hg burden in the region was first evaluated with multi-year observations of
903 air concentrations of Hg and seasonally accumulated Hg in snow. Model-measurement agreement
904 of Hg surface air concentrations and snow loadings in AOSR were within the measurement and
905 modeling uncertainties and implies that NPRI reported emissions of Hg from oil sands operations
906 (i.e., 59, 69, 44 and 25 kg in 2012, 2013, 2014 and 2015, respectively) are consistent with Hg
907 burden in the region. Air concentrations of Hg(0) in the AOSR (1.4 ng m^{-3}) were at a similar level
908 as found in Northern Alberta, and were within the range of concentrations in Canada ($1.2\text{-}1.6 \text{ ng m}^{-3}$).
909 Background Hg(0) concentrations in Canada are dominated by long-range transport, with a
910 slightly larger impact in the west, and, thus, contribution of oil sands activities to Hg(0)
911 concentrations in AOSR was minimal ($< 0.1\%$, average enrichment). During the summer season,
912 Hg emissions originating from regional wildfires were found to be an episodically important
913 source of atmospheric Hg(0), with daily averaged concentrations peaking to 2.5 ng m^{-3} (Parsons
914 et al. 2013; Fraser et al., 2018). Average total oxidized Hg concentrations (gaseous plus
915 particulate) in the air were elevated above background by 55% and 65% in 2012 and 2013,
916 respectively, and over 10% in 2015 within 50 km of upgrading facilities (particularly in the
917 northeast sector) in the AOSR as a result of oil sands emissions.



918

919 The level and spatial extent of the impact of oil sands emissions to winter, summer and annual Hg
920 deposition fluxes were examined in high (2012-2013) and low (2014-2015) oil sands Hg emission
921 years. In 2012-2015, annual average total Hg deposition fluxes of 15.6-18.3 $\mu\text{g m}^{-2}\text{y}^{-1}$) were
922 simulated in AOSR with deposition in winter (November-April) and summer (June-August)
923 contributing to 20% and 50%, respectively. The emission sources of Hg deposition in the AOSR
924 are global anthropogenic (including Canadian emissions), natural and reemissions of legacy Hg
925 deposition (including biomass burning emissions). Similar to other regions in Canada, on a broader
926 scale, Hg deposition in the AOSR is dominated by mercury transported from global sources, with
927 a small (and highly spatiotemporal variable) impact from regional biomass burning events. In
928 proximity to oil sands sources, however, total Hg deposition in wintertime was largely driven by
929 oils sands emissions. Deposition increases of up to 146-500% occurred within 10 km of oil sands
930 sources in the high emission years 2012 and 2013; summertime and annual Hg deposition increases
931 due to oil sands emissions were 13-56% and 24-70%, respectively, within 10 km of sources for
932 the same years. In lower oil sands emission years (2014 and 2015), Hg deposition increases due to
933 oil sands activities declined to 40-104% in winter and 5-14% annually within 10 km of oil sands
934 sources. At 20 km from the oil sands operations, oil sands-related Hg deposition enhancements
935 were not as large, with increases of 57-75% in winter, and 10% annually in 2012 and 2013. The
936 spatial extent of the OSE influence on Hg deposition was also greater in winter relative to summer
937 (~100 km vs 30 km from major Hg emitting facilities).

938

939 Finally, factors contributing to the inter-annual variations (i.e., changes in meteorological
940 conditions, oil sands emissions and wildfire emissions) in seasonal and annual Hg deposition
941 fluxes and relative source attributions in AOSR were examined from 2012 to 2015. Wintertime
942 (net) Hg deposition to northern landscapes is controlled by Hg deposition to snowpacks by direct
943 uptake and via snowfall and post-depositional processes, which exhibit strong inter-annual
944 variations. Relative to 2012, while changes in meteorological conditions led to a reduction in
945 wintertime Hg net deposition fluxes by ~ 17% in 2013-2014, and an increase by 10% in 2015
946 within 10 km of oil sands sources, changes in oil sands emissions led to deposition reductions of
947 10%, 35% and 56% in 2013, 2014 and 2015, respectively, resulting in an overall reduction in
948 wintertime Hg depositions of 27%, 52% and 46% in 2013, 2014 and 2015, respectively.



949 Gopalapillai et al. (2019) reported temporal decline in snowpack total Hg loadings near-field, from
950 an average load of 510 to 175 ng/m² from 2008 to 2016. At a distance of 10-20 km from the oil
951 sands sources, while changes in meteorology led to a 54% increase in wintertime deposition in
952 2015 relative to 2012, the decline in oil sands emissions led to a reduction in the deposition by
953 35%, resulting in an overall increase in Hg deposition of 19%. Summertime Hg deposition to
954 terrestrial systems is temporally less variable than wintertime deposition as it is predominantly
955 driven by Hg uptake by vegetation and soils, and by wet deposition; thus, changes in oil sands
956 emissions played a more significant role in summertime inter-annual variations in Hg deposition
957 than the meteorological factors. Compared to 2012, changes in meteorology, biomass burning and
958 oil sand emissions led to changes in summertime deposition by -3%, -2%, and +7% in 2013, +3%,
959 +2% and -15% in 2014, and -1%, +4% and -20% in 2015, resulting in overall changes in Hg
960 deposition by +2%, -10% and -17% in 2013, 2014 and 2015, respectively, within 10 km of major
961 oil sands sources. On an annual basis, in 2014 and 2015, variations in meteorology and biomass
962 burning emissions led to deposition increases of 1-6% and 2%, respectively, and reduction in oil
963 sands Hg emissions led to declines between 15-22%, resulting in an overall reduction in annual
964 Hg deposition of 7-20% within 10 km of AR6. In 2015, at 10-20 km away from sources, Hg
965 deposition increase due to changes in meteorology plus biomass burning was approximately equal
966 to deposition decline due to changes in oil sands emissions, resulting in smaller (<8%) changes in
967 Hg deposition fluxes.

968

969 Oil sands Hg emissions are found to be important sources of Hg contamination to the local
970 landscape in proximity of the processing activities, particularly in wintertime. Although Hg
971 deposition is higher in summertime (mainly driven by long-range transport), oil sands Hg
972 emissions contribute to a notably higher proportion of deposition in wintertime in the AOSR. Thus,
973 the impact of oil sands emissions is more easily detected in snow Hg observations (Kirk et al.,
974 2014). Wintertime Hg deposition rates are also more influenced by interannual changes in
975 meteorological conditions compared to summer. Regarding the environmental importance of
976 seasonal Hg deposition, it is likely that a major portion of summertime deposition remains bound
977 to vegetation and subsequently transferred to soils, where it can be partially sequestered and partly
978 reemitted back to air or mobilized in aquatic systems on long timescales of decades to centuries
979 (Zhou et al. 2021). In contrast, wintertime deposition (and partially summertime wet deposition)



980 can be transferred to the local aquatic system via runoff more readily (i.e, on an annual time scale).
981 Model findings reveal that year-to-year changes in meteorological conditions not only significantly
982 influence the rate of Hg deposition but, additionally, can either exacerbate or diminish the impact
983 of changes in oil sands emissions on Hg deposition, particularly in winter. Thus, meteorological
984 changes can confound the interpretation of trends in short-term monitoring data. In addition,
985 meteorological changes related to climate change can influence the deposition trends. Accurate
986 reporting of point and area Hg emisisions related to oil sands activities, long-term monitoring of
987 Hg in air and terrestrial ecosystems, and the application of process-based Hg models are crucial to
988 understanding systematic changes in Hg levels and their causes in the AOSR.

989

990 **Acknowledgements**

991 We thank our ECCC colleagues Paul Makar, Sandro Leonardelli and Stewart Cober and in the
992 Pollutant Inventory and Reporting Division for their insightful comments and careful internal
993 review of the manuscript. This project was supported by the Joint Oil Sands Monitoring (JOSM)
994 program of ECCC.

995

996

997 **References**

- 998 Alexander, A. C. and Chambers, P. A.: Assessment of seven Canadian rivers in relation to stages
999 in oil sands industrial development, 1972–2010, *Environmental Reviews* 24, 484–494,
1000 <https://doi.org/10.1139/er-2016-0033>, 2016.
- 1001 AMAP and UNEP: Technical Background Report for the Global Mercury Assessment 2013.
1002 Chapter 3. Atmospheric Pathways, Transport and Fate., 263, 2013.
- 1003 Angot, H., Dastoor, A., De Simone, F., Gårdfeldt, K., Gencarelli, C. N., Hedgecock, I. M.,
1004 Langer, S., Magand, O., Mastro Monaco, M. N., Nordstrøm, C., Pfaffhuber, K. A., Pirrone,
1005 N., Ryjkov, A., Selin, N. E., Skov, H., Song, S., Sprovieri, F., Steffen, A., Toyota, K.,
1006 Travnikov, O., Yang, X., and Dommergue, A.: Chemical cycling and deposition of
1007 atmospheric mercury in polar regions: review of recent measurements and comparison with
1008 models, *Atmospheric Chemistry and Physics* 16, 10735–10763,
1009 <https://doi.org/10.5194/acp-16-10735-2016>, 2016.



- 1010 APEI: Government of Canada, Air Pollutant Emissions Inventory,
1011 [https://www.canada.ca/en/environment-climate-change/services/pollutants/air-emissions-
1012 inventory-overview.html](https://www.canada.ca/en/environment-climate-change/services/pollutants/air-emissions-
1012 inventory-overview.html), accessed 25 Jul 2019
- 1013 Bieser, J., Slemr, F., Ambrose, J., Brenninkmeijer, C., Brooks, S., Dastoor, A., DeSimone, F.,
1014 Ebinghaus, R., Gencarelli, C. N., Geyer, B., Gratz, L. E., Hedgecock, I. M., Jaffe, D.,
1015 Kelley, P., Lin, C.-J., Jaegle, L., Matthias, V., Ryjkov, A., Selin, N. E., Song, S.,
1016 Travnikov, O., Weigelt, A., Luke, W., Ren, X., Zahn, A., Yang, X., Zhu, Y., and Pirrone,
1017 N.: Multi-model study of mercury dispersion in the atmosphere: vertical and
1018 interhemispheric distribution of mercury species, *Atmospheric Chemistry and Physics* 17,
1019 6925–6955, <https://doi.org/10.5194/acp-17-6925-2017>, 2017.
- 1020 Bloom, N. S. and Creelius, E. A.: Determination of mercury in seawater at sub-nanogram per
1021 liter levels, *Marine chemistry* 14, 49–59, [https://doi.org/10.1016/0304-4203\(83\)90069-5](https://doi.org/10.1016/0304-4203(83)90069-5),
1022 1983.
- 1023 CMSA: Canadian Mercury Science Assessment 2016, *Clean Air Regulatory Agenda*, 437–556,
1024 2016.
- 1025 Cooke, C. A., Kirk, J. L., Muir, D. C. G., Wiklund, J. A., Wang, X., Gleason, A., and Evans, M.
1026 S.: Spatial and temporal patterns in trace element deposition to lakes in the Athabasca oil
1027 sands region (Alberta, Canada), *Environmental Research Letters* 12,
1028 <https://doi.org/10.1088/1748-9326/aa9505>, 2017.
- 1029 Dastoor, A. P., Davignon, D., Theys, N., Van Roozendaal, M., Steffen, A., and Ariya, P. A.:
1030 Modeling dynamic exchange of gaseous elemental mercury at polar sunrise, *Environmental
1031 Science & Technology* 42, 5183–5188, 2008.
- 1032 Dastoor, A. P. and Durnford, D. A.: Arctic Ocean: Is it a sink or a source of atmospheric
1033 mercury?, *Environmental Science & Technology* 48, 1707–1717,
1034 <https://doi.org/10.1021/es404473e>, 2014.
- 1035 De Simone, F., Cinnirella, S., Gencarelli, C. N., Yang, X., Hedgecock, I. M., and Pirrone, N.:
1036 Model study of global mercury deposition from biomass burning, *Environmental science &
1037 technology* 49, 6712–6721, 2015.
- 1038 Durnford, D., Dastoor, A., Figueras-Nieto, D., and Ryjkov, A.: Long range transport of mercury
1039 to the Arctic and across Canada, *Atmospheric Chemistry and Physics* 10, 6063–6086,
1040 <https://doi.org/10.5194/acp-10-6063-2010>, 2010.



- 1041 Durnford, D., Dastoor, A., Ryzhkov, A., Poissant, L., Pilote, M., and Figueras-Nieto, D.: How
1042 relevant is the deposition of mercury onto snowpacks?—Part 2: A modeling study,
1043 Atmospheric Chemistry and Physics 12, 9251–9274, 2012.
- 1044 Eckley, C. S., Parsons, M. T., Mintz, R., Lapalme, M., Mazur, M., Tordon, R., Elleman, R.,
1045 Graydon, J. A., Blanchard, P., and St Louis, V.: Impact of closing Canada’s largest point-
1046 source of mercury emissions on local atmospheric mercury concentrations., Environ Sci
1047 Technol 47, 10339–10348, <https://doi.org/10.1021/es401352n>, 2013.
- 1048 Emmerton, C. A., Cooke, C. A., Wentworth, G. R., Graydon, J. A., Ryjkov, A., and Dastoor, A.:
1049 Total Mercury and Methylmercury in Lake Water of Canada’s Oil Sands Region., Environ
1050 Sci Technol 52, 10946–10955, <https://doi.org/10.1021/acs.est.8b01680>, 2018.
- 1051 EPA: United States Government: EPA Air Emissions Inventories, [https://www.epa.gov/air-](https://www.epa.gov/air-emissions-inventories)
1052 [emissions-inventories](https://www.epa.gov/air-emissions-inventories); accessed 25 Jul 2019
- 1053 EPA: Method 1669: Sampling ambient water for trace metals at EPA water quality criteria
1054 levels, 1996.
- 1055 Faïn, X., Helmig, D., Hueber, J., Obrist, D., and Williams, M. W.: Mercury dynamics in the
1056 Rocky Mountain, Colorado, snowpack, Biogeosciences 10, 3793–3807, 2013.
- 1057 Fraser, A., Dastoor, A., and Ryjkov, A.: How important is biomass burning in Canada to
1058 mercury contamination, Atmospheric Chemistry and Physics 18, 7263,
1059 <https://doi.org/10.5194/acp-18-7263-2018>, 2018.
- 1060 Friedli, H. R., Radke, L. F., and Lu, J. Y.: Mercury in smoke from biomass fires, Geophysical
1061 Research Letters 28, 3223–3226, 2001.
- 1062 GoC: Government of Canada, Historical Climate Data, <https://climate.weather.gc.ca>, accessed 19
1063 Feb 2019
- 1064 Gopalapillai, Y., Kirk, J. L., Landis, M. S., Muir, D. C. G., Cooke, C. A., Gleason, A., Ho, A.,
1065 Kelly, E., Schindler, D., Wang, X., and Lawson, G.: Source Analysis of Pollutant Elements
1066 in Winter Air Deposition in the Athabasca Oil Sands Region: A Temporal and Spatial
1067 Study, ACS Earth and Space Chemistry 3, 1656–1668,
1068 <https://doi.org/10.1021/acsearthspacechem.9b00150>, 2019.
- 1069 Graydon, J. A., St. Louis, V. L., Lindberg, S. E., Hintelmann, H., and Krabbenhoft, D. P.:
1070 Investigation of Mercury Exchange between Forest Canopy Vegetation and the



- 1071 Atmosphere Using a New Dynamic Chamber, *Environmental Science & Technology*
1072 40, 4680–4688, <https://doi.org/10.1021/es0604616>, 2006.
- 1073 Gustin, M. S., Huang, J., Miller, M. B., Peterson, C., Jaffe, D. A., Ambrose, J., Finley, B. D.,
1074 Lyman, S. N., Call, K., Talbot, R., Feddersen, D., Mao, H., and Lindberg, S. E.: Do We
1075 Understand What the Mercury Speciation Instruments Are Actually Measuring? Results of
1076 RAMIX., *Environmental Science & Technology* <https://doi.org/10.1021/es3039104>,
1077 2013.
- 1078 Gustin, M. S., Amos, H. M., Huang, J., Miller, M. B., and Heidecorn, K.: Measuring and
1079 modeling mercury in the atmosphere: a critical review, *Atmos. Chem. Phys.*, 15, 5697–
1080 5713, <https://doi.org/10.5194/acp-15-5697-2015>, 2015.
- 1081 Jia, L.: Oil Sands Bitumen Emulsion Upgrading by Using In Situ Hydrogen Generated through
1082 the Water Gas Shift Reaction, 2014.
- 1083 Kelly, E. N., Schindler, D. W., Hodson, P. V., Short, J. W., Radmanovich, R., and Nielsen, C.
1084 C.: Oil sands development contributes elements toxic at low concentrations to the
1085 Athabasca River and its tributaries, *Proceedings of the National Academy of Sciences* 107,
1086 16178–16183, <https://doi.org/10.1073/pnas.1008754107>, 2010.
- 1087 Kirk, J. L., Muir, D. C. G., Gleason, A., Wang, X., Lawson, G., Frank, R. A., Lehnerr, I., and
1088 Wrona, F.: Atmospheric deposition of mercury and methylmercury to landscapes and
1089 waterbodies of the Athabasca oil sands region, *Environmental science & technology* 48,
1090 7374–7383, 2014.
- 1091 Kos, G., Ryzhkov, A., Dastoor, A., Narayan, J., Steffen, A., Ariya, P. A., and Zhang, L.:
1092 Evaluation of discrepancy between measured and modelled oxidized mercury species,
1093 *Atmospheric Chemistry and Physics* 13, 4839–4863, [https://doi.org/10.5194/acp-13-4839-](https://doi.org/10.5194/acp-13-4839-2013)
1094 2013, 2013.
- 1095 Larter, S. R. and Head, I. M.: Oil sands and heavy oil: origin and exploitation, *Elements* 10, 277–
1096 283, 2014.
- 1097 Lynam, M., Dvonch, J. T., Barres, J., and Percy, K.: Atmospheric wet deposition of mercury to
1098 the Athabasca oil sands region, Alberta, Canada, *Air Quality, Atmosphere & Health* 11,
1099 83–93, 2018.



- 1100 Ma, J., Hintelmann, H., Kirk, J., and Muir, D.: Mercury concentrations and mercury isotope
1101 composition in lake sediment cores from the vicinity of a metal smelting facility in Flin
1102 Flon, Manitoba, Chemical Geology <https://doi.org/10.1016/j.chemgeo.2012.10.037>, 2012.
- 1103 Makar, P., Akingunola, A., Pabla, B., Stroud, C., Chen, J., Cheung, P., Moran, M., Gong, W.,
1104 Zheng, Q., and Li, S. M.: Experimental Forecasting Using the High-Resolution Research
1105 Configuration of GEM-MACH, International Technical Meeting on Air Pollution
1106 Modelling and its Application, 225–230, 2018.
- 1107 Muir, D.C.G., Wang, X., Yang, F., Nguyen, N., Jackson, T.A., Evans, M.S., Douglas, M., Kock, G.,
1108 Lamoureux, S., Pienitz, R., Smol, J.P., Vincent, W.F., Dastoor, A. (2009). ‘Spatial trends and historical
1109 deposition of mercury in eastern and northern Canada inferred from lake sediment cores.’ *Environment
1110 Science & Technology*, 43, 4802 – 4809.
- 1111
- 1112 NPRI: Government of Canada, Access the reporting guide for the National Pollutant Release
1113 Inventory, [https://www.canada.ca/en/environment-climate-change/services/national-
1114 pollutant-release-inventory/report/access-reporting-guide.html](https://www.canada.ca/en/environment-climate-change/services/national-pollutant-release-inventory/report/access-reporting-guide.html), accessed 25 Jul 2019
- 1115 NPRI: Government of Canada, National Pollutant Release Inventory, [https://www.ec.gc.ca/inrp-
1116 npri/](https://www.ec.gc.ca/inrp-npri/), accessed 25 Jul 2019
- 1117 Obrist, D., Johnson, D. W., and Edmonds, R. L.: Effects of vegetation type on mercury
1118 concentrations and pools in two adjacent coniferous and deciduous forests, *Journal of Plant
1119 Nutrition and Soil Science* 175, 68–77, <https://doi.org/10.1002/jpln.201000415>, 2012.
- 1120 Obrist, D. *et al.* A synthesis of terrestrial mercury in the western United States: Spatial
1121 distribution defined by land cover and plant productivity. *Science of the Total Environment*
1122 568, 522-535, doi:10.1016/j.scitotenv.2015.11.104 (2016).
- 1123 Parsons, M., McLennan, D., Lapalme, M., Mooney, C., Watt, C., and Mintz, R.: Total gaseous
1124 mercury concentration measurements at Fort McMurray, Alberta, Canada, *Atmosphere* 4,
1125 472–493, <https://doi.org/10.3390/atmos4040472>, 2013.
- 1126 Steffen, A. and Schroeder, W. H.: Standard Operating Procedures Manual Procedure for Total
1127 Gaseous Mercury Measurements-Canadian Atmospheric Mercury Measurement Network
1128 (CAMNet), Meteorological Service of Canada 4905, 1999.
- 1129 Travníkov, O., Angot, H., Artaxo, P., Bencardino, M., Bieser, J., D'Amore, F.,
1130 Dastoor, A., De Simone, F., Diéguez, M. D. C., Dommergue, A., Ebinghaus, R., Feng, X.



- 1131 B., Gencarelli, C. N., Hedgecock, I. M., Magand, O., Martin, L., Matthias, V., Mashyanov,
1132 N., Pirrone, N., Ramachandran, R., Read, K. A., Ryjkov, A., Selin, N. E., Sena, F., Song,
1133 S., Sprovieri, F., Wip, D., Wängberg, I., and Yang, X.: Multi-model study of mercury
1134 dispersion in the atmosphere: atmospheric processes and model evaluation, *Atmospheric*
1135 *Chemistry and Physics* 17, 5271–5295, <https://doi.org/10.5194/acp-17-5271-2017>, 2017.
- 1136 UN: Minamata Convention on Mercury, 72, 2017, <http://www.mercuryconvention.org>.
- 1137 UNEP: The Global Atmospheric Mercury Assessment: Sources, Emissions and Transport, 2008.
- 1138 UNEP: Global Mercury Assessment 2013, Sources, Emissions, Releases and Environmental
1139 Transport, 2013.
- 1140 UNEP: Global Mercury Assessment 2018, 2018.
- 1141 Wasiuta, V., Kirk, J. L., Chambers, P. A., Alexander, A. C., Wyatt, F. R., Rooney, R. C., and
1142 Cooke, C. A.: Accumulating Mercury and Methylmercury Burdens in Watersheds
1143 Impacted by Oil Sands Pollution., *Environ Sci Technol* 53, 12856–12864,
1144 <https://doi.org/10.1021/acs.est.9b02373>, 2019.
- 1145 Whaley, C. H., Galarneau, E., Makar, P. A., Akingunola, A., Gong, W., Gravel, S., Moran, M.
1146 D., Stroud, C., Zhang, J., and Zheng, Q.: GEM-MACH-PAH (rev2488): a new high-
1147 resolution chemical transport model for North American polycyclic aromatic hydrocarbons
1148 and benzene, *Geoscientific Model Development* 11, 2609–2632,
1149 <https://doi.org/10.5194/gmd-11-2609-2018>, 2018.
- 1150 Wiedinmyer, C., Akagi, S. K., Yokelson, R. J., Emmons, L. K., Al-Saadi, J. A., Orlando, J. J.,
1151 and Soja, A. J.: The Fire INventory from NCAR (FINN): A high resolution global model to
1152 estimate the emissions from open burning, *Geoscientific Model Development* 4, 625, 2011.
- 1153 Wiedinmyer, C. and Friedli, H.: Mercury emission estimates from fires: An initial inventory for
1154 the United States, *Environmental science & technology* 41, 8092–8098,
1155 <https://doi.org/10.1021/es071289o>, 2007.
- 1156 Willis, C. E., Kirk, J. L., St Louis, V. L., Lehnherr, I., Ariya, P. A., and Rangel-Alvarado, R. B.:
1157 Sources of Methylmercury to Snowpacks of the Alberta Oil Sands Region: A Study of In
1158 Situ Methylation and Particulates., *Environ Sci Technol* 52, 531–540,
1159 <https://doi.org/10.1021/acs.est.7b04096>, 2018.
- 1160 Willis, C. E., St Louis, V. L., Kirk, J. L., St Pierre, K. A., and Dodge, C.: Tailings ponds of the
1161 Athabasca Oil Sands Region, Alberta, Canada, are likely not significant sources of total



- 1162 mercury and methylmercury to nearby ground and surface waters., *Sci Total Environ* 647,
1163 1604–1610, <https://doi.org/10.1016/j.scitotenv.2018.08.083>, 2019.
- 1164 Wright, L. P., Zhang, L., and Marsik, F. J.: Overview of mercury dry deposition, litterfall, and
1165 throughfall studies, *Atmospheric Chemistry and Physics* 16, 13399,
1166 <https://doi.org/10.5194/acp-16-13399-2016>, 2016.
- 1167 Zhang, L., Wright, L. P. & Blanchard, P. A review of current knowledge concerning dry
1168 deposition of atmospheric mercury. *Atmospheric Environment* 43, 5853-5864, 2009.
- 1169 Zhang, J., Moran, M. D., Zheng, Q., Makar, P. A., Baratzadeh, P., Marson, G., Liu, P., and Li,
1170 S.-M.: Emissions preparation and analysis for multiscale air quality modeling over the
1171 Athabasca Oil Sands Region of Alberta, Canada, *Atmospheric Chemistry and Physics* 18,
1172 10459–10481, 2018.
- 1173 Zhang, L., Wu, Z., Cheng, I., Wright, L. P., Olson, M. L., Gay, D. A., Risch, M. R., Brooks, S.,
1174 Castro, M. S., Conley, G. D., Edgerton, E. S., Holsen, T. M., Luke, W., Tordon, R., and
1175 Weiss-Penzias, P.: The estimated six-year mercury dry deposition across North America,
1176 *Environ. Sci. Technol.*, 50, 12864–12873, <https://doi.org/10.1021/acs.est.6b04276>, 2016.
- 1177 Zhou, J., Obrist, D., Dastoor, A., Jiskra, M., and Ryjkov, A.: Vegetation uptake of mercury and
1178 impacts on global cycling, *Nature Reviews Earth & Environment*, 1-16,
1179 <https://doi.org/10.1038/s43017-021-00146-y>, 2021.
- 1180